# Structure-Based Prediction of G-Protein-Coupled Receptor Ligand Function: A β-Adrenoceptor Case Study

Albert J. Kooistra, Rob Leurs, Iwan J. P. de Esch, and Chris de Graaf*

Amsterdam Institute for Molecules, Medicines and Systems (AIMMS), Division of Medicinal Chemistry, Faculty of Science, VU University Amsterdam, De Boelelaan 1083, 1081 HV Amsterdam, The Netherlands

S *Supporting Information*

ABSTRACT: The spectacular advances in G-protein-coupled receptor (GPCR) structure determination have opened up new possibilities for structure-based GPCR ligand discovery. The structure-based prediction of whether a ligand stimulates (full/partial agonist), blocks (antagonist), or reduces (inverse agonist) GPCR signaling activity is, however, still challenging. A total of 31 β_1 (β_1R) and β_2 (β_2R) adrenoceptor crystal structures, including antagonist, inverse agonist, and partial/full agonist-bound structures, allowed us to explore the possibilities and limitations of structure-based prediction of GPCR ligand function. We used all unique protein–ligand interaction fingerprints (IFPs) derived from all ligand-bound β-adrenergic crystal structure monomers to post-process the docking poses of known β_1R/β_2R partial/full agonists, antagonists/inverse agonists, and physicochemically similar decoys in each of the β_1R/β_2R structures. The systematic analysis of these 1920 unique IFP–structure combinations offered new insights into the relative impact of protein conformation and IFP scoring on selective virtual screening (VS) for ligands with a specific functional effect. Our studies show that ligands with the same function can be efficiently classified on the basis of their protein–ligand interaction profile. Small differences between the receptor conformation (used for docking) and reference IFP (used for scoring of the docking poses) determine, however, the enrichment of specific ligand types in VS hit lists. Interestingly, the selective enrichment of partial/full agonists can be achieved by using agonist IFPs to post-process docking poses in agonist-bound as well as antagonist-bound structures. We have identified optimal structure–IFP combinations for the identification and discrimination of antagonists/inverse agonist and partial/full agonists, and defined a predicted IFP for the small full agonist norepinephrine that gave the highest retrieval rate of agonists over antagonists for *all* structures (with an enrichment factor of 46 for agonists and 8 for antagonists on average at a 1% false-positive rate). This β-adrenoceptor case study provides new insights into the opportunities for selective structure-based discovery of GPCR ligands with a desired function and emphasizes the importance of IFPs in scoring docking poses.
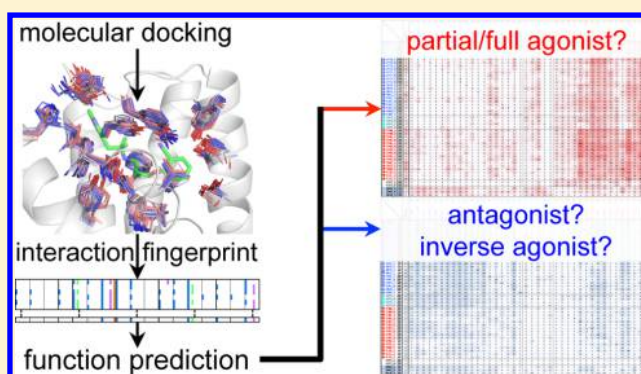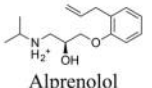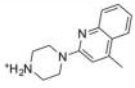
INTRODUCTION
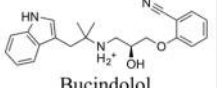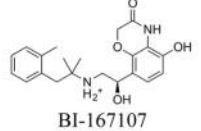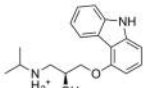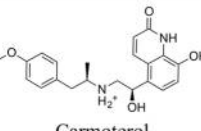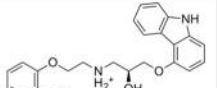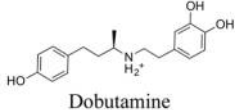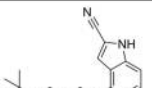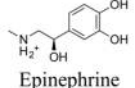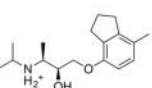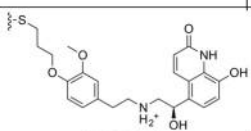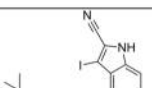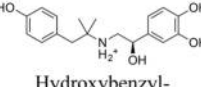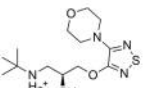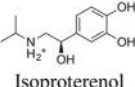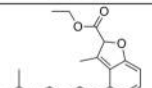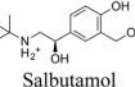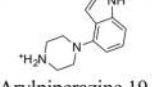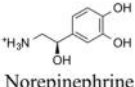
G-protein-coupled receptors (GPCRs) are versatile membrane-bound switch nodes of cell function and are arguably one of the most important classes of proteins that is encoded in the human genome.[1,2] GPCR ligands are able to stimulate (agonism), block (antagonism), or reduce (inverse agonism) the G-protein signaling activity of these receptor.[3–5] More recently, the fact that these GPCR ligands are able to (independently) modulate G protein-dependent but also G protein-independent pathways (via β-arrestin) has been getting more attention of the research community.[3–5] This new concept of biased signaling is an intriguing phenomenon, in which different ligands can promote or block multiple conformational states of the same receptor that are each linked to a different functional outcome.[4–8] The first human GPCR crystal structures were only solved in the past 7 years[9,10] and have substantially increased our understanding of the molecular details of how GPCRs work.[10–12] These spectacular advances

in GPCR structure determination have resulted in 115 crystal structures[13] at this moment, covering 21 class A,[9,10] 2 class B,[14,15] 2 class C,[16] and 1 class F[17] GPCRs. Despite these advances, less than 2% of all human GPCRs have been crystallized. Furthermore, most of these structures represent inactive-state conformations, with the exception of the adenosine A_{2A} receptor,[18] the neurotensin NTS_1 receptor,[19] and the β-adrenoceptors 1 (β_1R) and 2 (β_2R).[10] The 31 different β_1R/β_2R structures (while we were finalizing this manuscript, a 32nd, covalently bound, β-adrenergic structure was released[20]) cover multiple receptor activation states in combination with 19 ligands with different functional effects (Table 1 and Supporting Information, Table S1).[21–35] This GPCR structure–function data set offers a unique opportunity to assess the possibilities and limitations of the structure-based

Table 1. Overview of All β-Adrenoceptor Crystal Structures, the Co-crystallized Ligands, and Their Function

PDB	Ligand	Function[a]	Bias[e]	Icon[p]	PDB	Ligand	Function[a]	Bias[e]	Icon[p]
3NYA[26]	Alprenolol	ANT	Yes[j] No[f,i,k]	▽ (blue)	3ZPR[34]	Arylpiperazine 20	ANT[b]	-	● (cyan)
4AMI[32]	Bucindolol	ANT[o]	Yes[g,m]	▽ (blue)	3P0G[28,q] 3SN6[29,q] 4LDE[75,q]	BI-167107	fAGO	Yes[n]	▼ (red)
2YCW[27] 2RH1[21] 4GBR[33] 2R4R[22,d] 2R4S[22,d] 3KJ6[25,d]	Carazolol	iAGO[o]	No[h]	● (blue)	2Y02[31]	Carmoterol	fAGO	Yes[m,n]	▼ (red)
4AMJ[32]	Carvedilol	iAGO	Yes[g,j,m] No[f]	▽ (blue)	2Y00[31] 2Y01[31]	Dobutamine	pAGO	Yes[f,r,s] No[l]	▼ (red)
2VT4[24] 2YCX[27] 2YCY[27] 4BVN[77]	Cyanopindolol	ANT[o]	-	● (blue)	4LDO[75,q]	Epinephrine	fAGO	No[f,g,l]	● (red)
3NY8[26]	ICI 118,551	iAGO	No[f,h]	● (blue)	3PDS[30,c]	FAUC50	fAGO	-	● (red)
2YCZ[27]	Iodocyanopindolol	ANT	-	● (blue)	4LDL[75,q]	Hydroxybenzyl-isoproterenol	fAGO	Yes[n]	▼ (red)
3D4S[23]	Timolol	iAGO	No[f]	● (blue)	2Y03[31]	Isoproterenol	fAGO	No[f,g,h,i j,k,l]	● (red)
3NY9[26]	VS hit (Kolb)	iAGO	-	● (blue)	2Y04[31]	Salbutamol	pAGO	No[l]	● (red)
3ZPQ[34]	Arylpiperazine 19	ANT[b]	-	● (cyan)	-	Norepinephrine	fAGO	No[g]	● (red)
4GPO[35]	Ligand-free								

[a]Function abbreviations, based: ANT, antagonist; AGO, agonist; i, inverse; p, partial; f, full. [b]Not validated.[34] [c]Covalently bound ligand. [d]Ligand and extracellular part of the receptor were not resolved due to weak electron density. [e]This column indicates whether a ligand has a signaling preference for the β-arrestin over the G-protein pathway or not according to the following references: [f]Casella et al.,[78] [g]Drake et al.,[79] [h]Kahsai et al.,[80] [i]Kaya et al.,[81] [j]Kim et al.,[82] [k]Liu et al.,[83] [l]Rajagopal et al.,[84] [m]Warne et al.,[32] and [n]Weiss et al.[52] [o]Although these ligands are generally considered as antagonists/inverse agonists, they can also have a partial agonist effect depending on the activation state of the receptor.[85,86] [p]Color coding: red, full/ partial agonist; blue, antagonist/inverse agonist; cyan, unvalidated antagonist. Ligands with a circle icon do not show a signaling preference or it is not known for these compounds; ligands with a triangle icon have been shown to have a β-arrestin signaling bias. [q]The receptor is in its active state. [r]The signaling bias is subtype specific according to Casella et al.[78] [s]The observed difference between the signaling pathways was small for these ligands. More information regarding the pharmacological properties of the co-crystallized ligands is detailed in Table S1.

computational prediction of GPCR ligand function (agonism, antagonism, and inverse agonism) in virtual screening (VS) studies, as such a set of crystal structures has never been available for GPCRs before.

GPCR crystal structures[18,36−41] and homology models[42,43] have been successfully used to discover new GPCR ligands.[2] While in most VS studies new antagonists were found by docking into inverse agonist/antagonist-bound GPCR crystal structures[36−41] or GPCR models based on the inactive bovine rhodopsin (bRho) structure[44] and refined using known antagonists,[42,43] several reports show that also agonists can be found by structure-based VS in inactive GPCR models.[45−50] In some of these studies,[48−50] the initial bRho-based inactive state homology model was refined using true agonists, but in other cases[45,46] the inactive model was refined using antagonists. Similarly, agonist-biased models have also been successfully applied to discover new antagonists.[47] More recently, a structure-based VS for A_{2A} *agonists* based on an active-state *agonist*-bound crystal structure resulted in the identification of 9 high-affinity adenosine *antagonists*, illustrating that the identification of novel ligands with the desired functional effect is challenging.[18] Possible reasons for this discrepancy between the (modeled) activation state of the GPCR structure used for docking and the functional activity of the VS are the limited understanding of the structural details of the receptor activation mechanism and associated ligand binding mode, inaccuracies in docking scoring functions, or a chemical bias toward ligands with a specific functional effect in the screened library.[18,51,52]

Previous docking-based VS studies against β_2R crystal structures nevertheless indicated that the functional activity of *in silico* hits is the same as the functional activity of the co-crystallized ligand bound to the structure that is used for the docking simulations.[53] While docking against the first carazolol (antagonist/inverse agonist)-bound β_2R crystal structure enabled the discovery of new β-adrenergic antagonists/inverse agonists,[40,54] docking studies against the BI167107 (full agonist)-bound active-state crystal structure facilitated the identification of partial/full agonists.[52] Moreover, even before the determination of partial/full agonist-bound β_2R crystal structures,[28−30] several studies showed that the inverse-agonist-bound β_2R crystal structure could be used for the selective identification of agonists by introducing (small) conformational changes in the β_2R structure and using customized scoring approaches to select docking poses.[55−58] In independent modeling studies,[55−58] the position and/or orientation of the side chains of S204[5.43] and S207[5.46] (through rotation of TM5 and/or adjustment of the rotameric states of S204[5.43] and S207[5.46]) was customized on the basis of ligand structure−activity relationship (SAR) and receptor mutation studies,[59−64] thereby enabling the preferential scoring of agonists over antagonists. The selective identification of partial/full agonists was significantly increased by employing an interaction fingerprint (IFP)[65] scoring method that determines ligand-binding-mode similarity instead of classical (energy-based) scoring functions.[55] These proof-of-concept studies illustrate how (small) differences in protein conformation can influence structure-based VS results, as has also been demonstrated by recent comparative VS studies against GPCR crystal structures and homology models.[11,12,34,37] Systematic consideration of alternative protein conformations/flexibility in docking simulations can, for example, be done either by incorporating flexibility for (selected) binding-site residues during the docking simulations,[66,67] by creating binding-site ensembles,[68] by using multiple crystal structures,[69] or by refining protein models with different ligands.[42,70,71]

GPCR crystal structure-based identification of new ligands with a different functional effect than the co-crystallized ligand has been defined as one of the challenges in the current era of GPCR structural and chemical biology.[11] The growing number of β-adrenoceptor crystal structures meanwhile covers multiple activation states and multiple co-crystallized ligands with different functional efficacies.[2,5,72] This unique GPCR structure−function data set allowed us, for the first time, to systematically and separately investigate the effects of both the reference ligands and the receptor conformations in combination with classical (energy-based)[53,73] and IFP scoring[65,74] approaches on the basis of GPCR crystal structures. In this study, we have investigated whether (and to what extent) (i) the crystal structures retain their preference for ligands with the same functional effect (agonism, antagonism, and inverse agonism) as the co-crystallized ligand, (ii) the different binding site conformations of the crystal structures have an impact on the outcome of VS studies, (iii) specific IFPs can change or amplify the preference of a crystal structure for ligands with a specific functional effect, (iv) the IFP derived from the predicted docking pose of a small agonist (norepinephrine) can be used for the selective retrieval of partial/full agonists (p/fAGO) over antagonist/inverse agonists (ANT/iAGO) and decoys, and (v) sufficient consistent pharmacological data are available to train structure-based VS models to accurately predict *biased* signaling of GPCR ligands.

■ RESULTS AND DISCUSSION

Subtle Ligand-Type-Dependent Structural Changes in the Receptor Binding Sites. We have analyzed 31 β-adrenergic structures: 15 human β_2R and 16 turkey β_1R structures (Table 1).[21−35,75] While we were finalizing this manuscript, a 32nd β-adrenergic structure was released[20] with a covalently bound agonist that forms similar H-bond interactions with TM5 as epinephrine (PDB code 4LDO)[75] and has the same covalent linker as FAUC50 (PDB code 3PDS).[30] Multiple crystallization methods have been employed to obtain stable crystals for structure determination of these receptor−ligand complexes,[9] among them T4 lysozyme insertion at the intracellular loop (ICL) 3 or at the N-terminus, introduction of thermostabilizing mutations, introduction of covalently binding ligands, and addition of antibody fragments.[76] All crystal structures were obtained in combination with one of the 19 unique ligands (apart from the ligand-free structure,[35] see Tables 1 and S1): 9 (partial/full) inverse agonists or antagonists, 7 (partial/full) agonists, 1 covalently bound full agonist, and 2 unvalidated fragments (but suggested to be antagonists,[34] *vide infra*). The functional effect of the cocrystallized ligands (Table 1) has been assigned in line with the functional classification as indicated in the first publication describing their co-crystallization (except for bucindolol, see footnotes in Table 1). It should be noted that this classification nearly always coincides with the way these compounds modulate the G-protein signaling pathway (Table S1). Throughout this article, we abbreviate full and partial agonists as f/pAGO, antagonists as ANT, and (full/partial) inverse agonists as iAGO (see legend in Table 1).

It should be noted that we do not focus on the differences between β_1R and β_2R in this article, as the pocket-lining residues are almost identical (only residue 7.35 differs, a phenylalanine in β_1R but tyrosine in β_2R), we assume that the
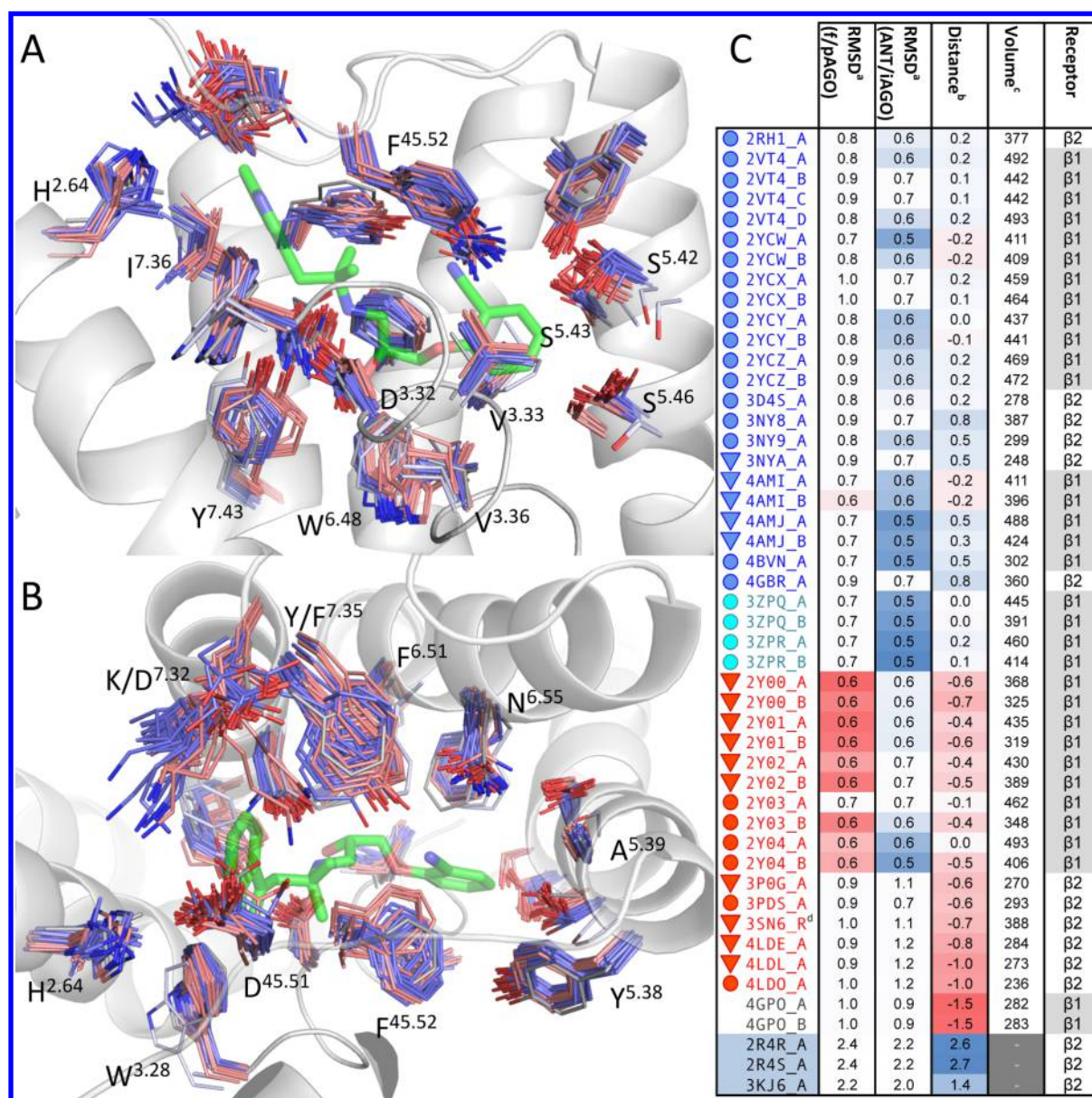
Figure 1. (A,B) Visual and (C) quantitative comparisons of the pockets from all X-ray structures. Pocket residues (carbon atoms are colored blue, salmon, white, and gray for ANT/iAGO, f/pAGO, FAB-complexed, and ligand-free structures, respectively) of all chains of all crystal structures (listed in panel C by their PDB code followed by their chain identifier) are shown superimposed with the cartoon representation of β_2R (PDB code 2RH1[21]) and bucindolol (green carbon atoms, PDB code 4AMI[32]), as seen from the side (panel A) and from the top (panel B). Panel C gives an overview of [a]average all-atom rmsd using the pocket residues (Å) compared to all 16 f/pAGO and all 27 ANT/iAGO structures (full overview in Supporting Information, Figure S2); [b]the average Z-score of the distances between G[2.61], D[3.32], N[7.39], and S[5.42] (full overview in Supporting Information, Figures S3 and S4); and [c]the pocket volume (Å[3], Supporting Information, Figure S5). [d]The side chains of the ECL2 residues are not all fully resolved, thereby influencing the pocket volume (Figure S5) as well as rmsd values. The red and blue background coloring mark values associated with f/pAGO and ANT/iAGO properties, respectively. Icons represent f/pAGO (red), ANT/iAGO (blue), or unvalidated ANT (cyan) with no or unknown signaling preference (circles) or β-arrestin-biased ligands (triangles) (see Table 1).

ligand-binding modes in β_1R and β_2R are transferable.[87] Also, in the set of ligands that we analyzed there is only one highly selective compound (ICI 118,551, which has a ~540-fold higher affinity for β_2R than for β_1R).[88] Moreover, it is suggested that selectivity for one of the receptors[78,85,88] is based on ligand kinetics[89] (i.e., binding to and dissociation from the receptor) and receptor activation[87] rather than differences in ligand binding modes.[89]

Superposition of all individual monomers of the crystal structures of β_1R and β_2R on the basis of their pocket residues (Figure 1) shows the conserved heptahelical fold (Supporting

Information, Figure S1) but also indicates some structural variation, in particular in TM1 (a 60° kink),[24,27] TM5, and TM6 (which differ between active and inactive states[28,29] and the straight and bent inactive-state TM6[27]). While the structural differences in the intracellular regions have been described in several reviews,[10,12] our systematic analysis will focus on the structural variations in the ligand-binding site within the β-adrenergic GPCR family. Figure 1A,B shows that the pocket residues in all (β_1R and β_2R) crystal structures have largely conserved conformations. The outliers are the FAB complexes (PDB codes 2R4R, 2R4S,[22] and 3KJ6[25]) in which
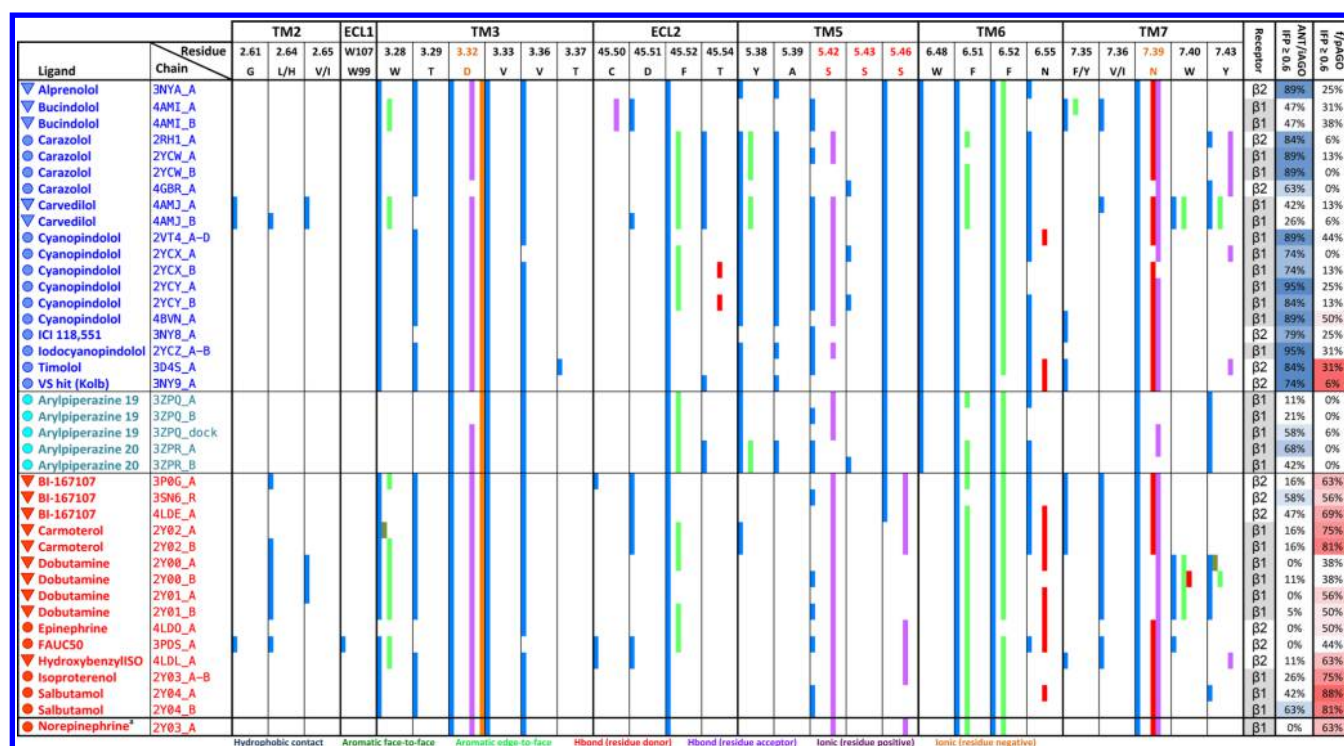
Figure 2. Overview of the unique interaction fingerprints of all cocrystallized ligands. The colors indicate the presence of an interaction (as seen from the residue) according to the colors described at the bottom of the figure. Identical IFPs for multiple monomers within a PDB entry are grouped (e.g., 2VT4_chainA-D). The last two columns describe the amount of times (as a percentage of the total comparisons) an IFP comparison results in a score ≥0.6 when compared with the ANT/iAGO reference IFPs (a blue background indicates a high percentage) and the f/pAGO reference IFPs (a red background indicates a high percentage). [a] The IFP of the highest scoring docking pose of norepinephrine in 2Y03-chainA (see Figure 6). Names and icons represent f/pAGO (red), ANT/iAGO (blue), or unvalidated ANT[34] (cyan) with no or unknown signaling preference (circle) or β-arrestin-biased ligands (triangle) (see Table 1).

the ECL domain, the top of the helices, and the ligand (carazolol) were not solved due to the distorted density in this region.[22,25] When comparing the pocket residues by means of the mutual root-mean-square deviation (rmsd) values (Figure 1C and Supporting Information, Figure S2), they are generally low (average all-atom rmsd 0.9 Å). By determining the average rmsd of the binding site residues of each individual structure to all f/pAGO and all ANT/iAGO structures, it becomes apparent that all f/pAGO structures and all inactive-state ANT/iAGO structures cluster together (Figure 1C). This means that the binding site conformation within the inactive-state f/pAGO structures, but also within the ANT/iAGO structures is conserved.[8] Moreover, the active-state structures form a separate cluster compared to other f/pAGO structures, which can be ascribed to the movement of TM5 and TM6[28,29] (Table 1, Figures S1 and S2).[90] Outliers are the FAB complexes (due to the distorted electron density), but also the ligand-free structure (PDB code 4GPO[35]), which have a high rmsd value compared to the other structures. Interestingly, this apo structure does not cluster with any of the f/pAGO structures or with ANT/iAGO structures.

To further quantify the differences between the pockets, we measured the distances between the Cα atoms of $G^{2.61}$, $D^{3.32}$, $N^{7.39}$, and $S^{5.42}$ (Figure 1C and Supporting Information, Figures S3 and S4). While the measurements show contraction of the pocket upon agonist binding[31] (mainly through movement of TM5), the highest contraction of the pocket was found for the ligand-free β_1R structure.[35] Note, however, that these differences are small and that mainly the distance between $D^{3.32}$ and $N^{7.39}$ to $S^{5.42}$ varies between the different structures (on average

0.6 and 1.0 Å, respectively). Analysis of volumes of the individual binding pockets (Figure 1C and Supporting Information, Figure S5) indicates that β_1R generally has a bigger pocket volume than β_2R (on average 415 Å[3] compared to 308 Å[3]). This can mainly be ascribed to the residue differences at positions 7.32 (D/K in β_1R/β_2R, respectively) and 7.35 (F/Y in β_1R/β_2R, respectively) resulting in a more confined ligand-binding space in β_2R (Figures 1 and S5). Although the rmsd values between all pocket residues are low (Figure 1C and Supporting Information, Figure S2), the effect of all subtle changes combined is reflected by the large differences in the pocket volumes. For the β_1R and β_2R the pocket volumes range from 282 to 493 Å[3] and from 236 to 388 Å[3], respectively (only comparing structures with fully resolved pocket residues). In line with the results of the distance measurements and the rmsd calculations, the ligand-free structure has the smallest pocket volume of all β_1R structures. The active-state epinephrine-bound structure (PDB code 4LDO[75]) has the smallest pockets volume of all β_2R structures, adapted to this small endogenous agonist.

Identification of Ligand-Type-Specific Molecular Interaction Profiles. The binding modes and interaction profiles of the 19 different co-crystallized ligands (Table 1 and Figure 2) were subsequently investigated using the aforementioned IFP method.[65] Like other protein−ligand interaction fingerprinting methods (e.g., PLIF,[91] SIFt,[92] and TIFP[93]), the IFP method has been used to improve the selection and scoring of docking poses for binding mode prediction and VS purposes, and has been successfully applied in both retrospective and prospective VS studies[38,42,45,94−98]
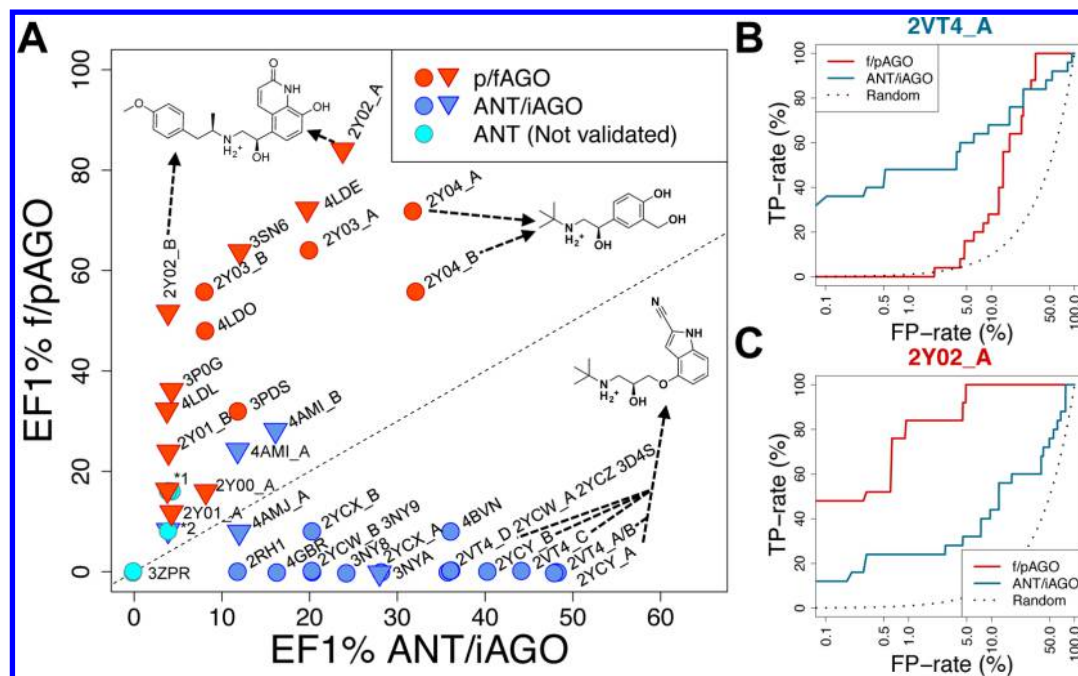
Figure 3. Overall enrichment at 1% false positive rate (FP-rate) for the retrieval of 25 partial/full agonists and 25 inverse agonists/antagonists over a set of 980 decoy molecules using IFP scoring (A). Full ROC curves visualizing the retrieval rate (TP-rate) of f/pAGO (red) and ANT/iAGO (blue) in the best ANT/iAGO structure (B) and best f/pAGO structure (C, legend shown in panel B). The structures are indicated by their PDB code followed by an underscore and the chain identifier (except when there was only one chain or all chains of the structure had similar performance). The 2D structures represent the co-crystallized ligand for selected structures. The ANT/iAGO axis is scaled from 0 to 60 and the f/pAGO axis from 0 to 100. *1 = 3ZPQ_A, 3ZPQ_dock, 2Y00_B; *2 = 4AMJ_B, 3ZPQ_B. Icons represent f/pAGO (red), ANT/iAGO (blue), or unvalidated ANT[34] (cyan) with no or unknown signaling preference (circle) or β-arrestin-biased ligands (triangle) (see Table 1).

(including the discovery of new histamine H_1 receptor,[38] histamine H_4 receptor,[99] and glucagon receptor[45] ligands). This technique encodes 7 different types of interactions between the ligand and each of the binding pocket residues. The following interactions with the ligand are encoded: hydrophobic contact, aromatic face-to-edge and face-to-face, H-bond acceptor–donor and donor–acceptor, and negative–positive and positive–negative ionic interactions (as shown in Figure 2).[65] The IFPs for all ligands in all monomers were calculated for the available β-adrenergic crystal structures. The 31 crystal structures contain in total 48 monomers (43 ligand-bound). Of the 14 crystallized ligand–protein complexes containing more than one monomer, only 3 structures had identical interaction patterns within different monomers of the same crystal structure (see Figure 2). Moreover, ligands present in multiple co-crystal structures (e.g., cyanopindolol, carazolol, BI-167107) did also not yield identical IFPs. This emphasizes once more that crystal structures are snapshots in time[100] of entities that are flexible by nature.

The overview of all generated reference IFPs from the ligand-bound crystal structures (Figure 2) shows that there are several conserved interactions within the pocket. Apart from dobutamine and arylpiperazines 19 and 20, all co-crystallized β_1R and β_2R ligands contain an ethanolamine moiety (which is abundant in β-adrenergic ligands[101]) that can form a tight H-bond interaction network with the side chains of $D^{3.32}$ and $N^{7.39}$ (Figure 2).[59,102] In chain B of the arylpiperazine 19 structure the ligand does not form H-bonds with $N^{7.39}$ nor with $D^{3.32}$. We therefore redocked the co-crystallized ligand into its structure considering alternative ring conformations, resulting in an additional IFP (annotated as *3ZPQ_dock*, see Figure 2, Supporting Information, Figure S6, and Materials and

Methods). Most β-adrenergic ligands contain an H-bond donor with which they are able to interact with S211/S203[5.42] (74%, Figures 2 and S7).[87] More specific for full agonists (carmoterol, isoproterenol, BI-167107, and FAUC50) is a catechol or a catechol-mimicking moiety with two (or more) H-bond donors that allows for an extra H-bond with another TM5 serine, namely S215/S207[5.46].[103] Partial agonists also have two H-bond donors that can interact with TM5, but their interactions seem to be less optimal (e.g., the shortest observed distance between the H-bond donor from the catechol in dobutamine to the $S^{5.46}$ acceptor is 3.8 Å).[87] All ligands also contain at least one aromatic ring, which allows for aromatic stacking with F307/F290[6.52], F306/F289[6.51], and F201/F193[45.52] in 95%, 56%, and 54% of all structures, respectively.

We furthermore observed aromatic interactions with W117/W109[3.28] for many agonists (60%), ionic interactions with the key ionic anchor D121/D113[3.32] for all ligands, and double H-bond interactions with N329/N312[7.39] as described above (see Figure S7).

All interaction profiles (IFPs) of co-crystallized ligands (8 f/pAGO and 11 ANT/iAGO) in 33 β_1R and 15 β_2R binding sites were compared, and their Tanimoto similarity scores were determined (Supporting Information, Figure S8). Figure 2 reports for each individual IFP the percentage of similar IFPs (Tanimoto similarity score ≥0.6[65]) derived from (other) ANT/iAGO and f/pAGO co-crystal structures complexes. This analysis shows that the IFPs of ANT/iAGO ligands are more similar to each other than to f/pAGO IFPs (75% versus 19% similar pairs, respectively). Vice versa, the pairwise similarity between f/pAGO IFPs is higher (62%) than similarity to ANT/iAGO (62% versus 21%, respectively, Figure 2). Moreover, the

Figure 4. Enrichment factors at a 1% false positive rate using all reference IFPs (columns) on all β-adrenergic monomers for the retrieval of for f/pAGO (A) and ANT/iAGO (B) over physicochemically similar decoys. The white to red and white to blue gradients as background color mark a low to high enrichment for f/pAGO (A) and ANT/iAGO, respectively. Icons represent f/pAGO (red), ANT/iAGO (blue), or unvalidated ANT[34] (cyan) with no or unknown signaling preference (circle) or β-arrestin-biased ligands (triangle) (see Table 1).

Figure 5. Analysis of VS runs using the IFPs (D,E) and structures (F,G) of the most f/p AGO-selective (2Y02_A) and ANT/iAGO-selective (2VT4_A) protein−ligand complexes (see Figure 3A), showing that both the reference IFP and protein structure determine enrichment and functional selectivity of the VS study. The binding modes of the selected f/pAGO (A, 2Y02_A) and selected ANT/iAGO (B, 2VT4_A) protein−ligand complex, a docked ligand with the same efficacy class (green carbon atoms), and their corresponding IFPs (C) for the displayed residues. $EF_{1\%}$ results for agonists and antagonist versus the decoys when using the reference IFP of the selected f/pAGO (D) and selected ANT/iAGO (E) for scoring docked compounds in all 48 protein structures. $EF_{1\%}$ results for f/pAGO and ANT/iAGO versus the decoys when using the 38 unique reference IFPs of all ligand−protein complexes for rescoring the docked compounds in the 2Y02_A (F) and 2VT4_A (G) structure. Icons represent f/pAGO (red), ANT/iAGO (blue), or unvalidated ANT[34] (cyan) with no or unknown signaling preference (circle) or β-arrestin-biased ligands (triangle) (see Table 1).

arylpiperazine ligands cluster together with the ANT/iAGO IFPs (on average 40% similar pairs compared to 1% similarity with f/pAGO IFPs) suggesting that that these compounds are antagonists, as previously proposed.[34] These analyses show that the functional effect of a ligand is encoded in the ligand–protein interaction patterns and suggest that these IFPs can be used to discriminate ANT/iAGO from f/pAGO ligands in structure-based VS studies.

Selective Retrieval of f/pAGO over ANT/iAGO in Structure-Based Virtual Screening. In order to quantify to what extent the differences between the individual structures and the reference IFPs have an influence on the outcome and selectivity of a VS, we docked a set of 1030 compounds comprising 25 f/pAGO (Supporting Information, Figure S9A), 25 ANT/iAGO (Figure S9B), and 980 physicochemically similar decoys[55] in all β_1R and β_2R structures. The docking studies were performed using PLANTS[104] using the ChemPLP scoring function, and the resulting binding modes were postprocessed using IFP[65] and ranked according to their PLANTS and IFP scores. Figure 3 shows that overall the ANT/iAGO ligand–protein complexes are more selective (average $EF_{1\%}$ = 27 and 4 for ANT/iAGO and f/pAGO, respectively) than the f/pAGO complexes (average $EF_{1\%}$ = 13 and 46 for ANT/iAGO and f/pAGO, respectively). However, VS against f/pAGO-bound structures in many cases gives a high enrichment for ANT/iAGO and an even higher enrichment for p/fAGO ligands. For example, VS against chain A of the salbutamol-bound β_1R structure (PDB code 2Y04) results in a remarkably high enrichment factor for both f/pAGO and ANT/iAGO ($EF_{1\%}$ = 72 and 32, respectively).

For 36 of the 43 protein–ligand complexes, the $EF_{1\%}$ of ligands with the *same* functional effect as the co-crystallized ligand was higher than the enrichment of ligands with a different functional effect (Figure 3). VS runs against five (putative) ANT/iAGO-bound receptor structures, namely the arylpiperazine-19-bound β_1R complexes (3ZPQ), the bucindolol-β_2R complexes (4AMI), and one of the carvedilol-β_2R complexes (4AMJ), resulted in a higher enrichment for p/fAGO ligands than for ANT/iAGO ligands. For the arylpiperazine-20-bound β_1R structures[34] (PDB code 3ZPR) no enrichment was obtained for any of the known ligands ($EF_{1\%}$ = 0).

In 85% of all f/pAGO and ANT/iAGO structures, IFP scoring yielded equal or higher enrichment factors ($EF_{1\%}$) compared to ChemPLP-scoring (Figure 4 and Supporting Information, Figure S10). Using IFP to rank the docking poses of ligands of the same functional activity class gives a VS enrichment that is on average 2 times as high as the enrichment obtained by ChemPLP-scoring. Moreover, in 90% of the structures IFP scoring yielded an equal or higher selectivity (higher retrieval of f/pAGO than ANT/iAGO over decoys for f/pAGO structures and vice versa) than when using ChemPLP scoring (Figures 4 and S10). The resulting $EF_{1\%}$ values of f/pAGO and ANT/iAGO based on IFP similarity scoring (using the co-crystallized ligand reference IFP) are shown in Figure 4A.

For 11 unique crystal structures (of the 14 structures with multiple monomers) a significant difference in the $EF_{1\%}$ is observed ($\Delta EF_{1\%} > 5$) between the individual monomers, demonstrating the impact of subtle differences in the reference IFP and/or binding site structure in different monomers of the same crystal structure. For example, the $EF_{1\%}$ for f/pAGO over decoys for chain A of structure 2Y02 is 84 compared to 52 for

chain B, while the reference IFPs of both chains is identical. This can potentially be ascribed to the larger pocket volume of chain A (490 versus 389 Å³ for chain B, which is mainly due to the rotation of F325[7.35]), therefore the pocket of chain A is better able to accommodate the larger ligands. In contrast, the small pocket of the ligand-free β_1R structure[35] (PDB code 4GPO) is not able to effectively accommodate ligands as D121[3.32], F307[6.52], and N329[7.39] are moved inward (Figure S5), thereby preventing the prediction of correct binding modes using rigid-protein docking simulations. Similarly, the small pocket of the active-state, epinephrine-bound β_2R structure (PDB code 4LDO[75]) is not able to accommodate the relatively bigger TM5/6 binding moieties of most ANT/iAGO and is therefore more selective for f/pAGO.

To evaluate the individual contribution of the reference IFPs and the protein structure, we rescored all docked compounds in all structures with all reference IFPs (i.e., not only with the IFP that was derived from the corresponding receptor–ligand complex). This furthermore allowed us to rescore the docked compounds with IFP in the structures without a ligand (PDB codes 2R4R, 2R4S, 3KJ6, and 4GPO). The resulting scoring matrices containing the $EF_{1\%}$ of f/pAGO and ANT/iAGO are shown in Figure 4A,B.

In Figure 4A, we see that also ANT/iAGO structures can be used to efficiently retrieve f/pAGO ligands when using the right reference IFP. This is surprising, as this contrasts the results of the previous VS studies in which the rotamers of the TM5 serines and/or whole TM5 had to be rotated for the efficient retrieval of f/pAGO ligands.[55−58] Interestingly, the isoproterenol IFP (PDB code 2Y03) allows efficient retrieval of f/pAGO ligands in all ANT/iAGO structures with an average $EF_{1\%}$ = 47. Ranking docking poses in f/pAGO structures with an ANT/iAGO reference IFP, on the other hand, does not yield high enrichments of ANT/iAGO ligands (with an average ANT/iAGO $EF_{1\%}$ = 13). The highest average $EF_{1\%}$ (= 21) was obtained by the cyanopindolol IFP (2YCY_B) in the f/pAGO structures.

An unanticipated finding was that when pairing *specific* f/pAGO IFPs with ANT/iAGO structures also high $EF_{1\%}$ values were obtained for the selective retrieval of ANT/iAGO. When the IFPs of salbutamol (pAGO, PDB code 2Y04) were used, an average ANT/iAGO $EF_{1\%}$ = 27 was obtained (Figure 4). In short, these statistics emphasize that not only the choice of structure but also the choice of reference IFP has a high impact on the resulting enrichment factors and, more interestingly, on the ligand selectivity of the results.

Selective Structure-Based Virtual Screening for Ligands with the Desired Functional Effect. On the basis of the highest $EF_{1\%}$ values (Figure 3), we selected one f/pAGO and one ANT/iAGO ligand–protein complex for a more detailed investigation. From all ANT/iAGO-bound complexes the cyanopindolol-bound (iAGO) β_1R structure 2VT4 (both chains A and B) obtained the highest ANT/iAGO $EF_{1\%}$ value (= 48) and a f/pAGO $EF_{1\%}$ value of 0. As both chains gave similar VS enrichments (Figure 4B), we randomly selected chain A of 2VT4 (Figure 5B/C) for further investigation. From all f/pAGO complexes, chain A of the carmoterol (fAGO)-bound structure β_1R structure 2Y02 (Figure 5A/C) obtained the highest f/pAGO $EF_{1\%}$ value (= 84) and an ANT/iAGO $EF_{1\%}$ value of 24. However, it should be noted that chain B of the 2Y02 structure and the active-state 3P0G structure also obtained high f/pAGO $EF_{1\%}$ values (= 52 and 36, respectively) with a much lower ANT/
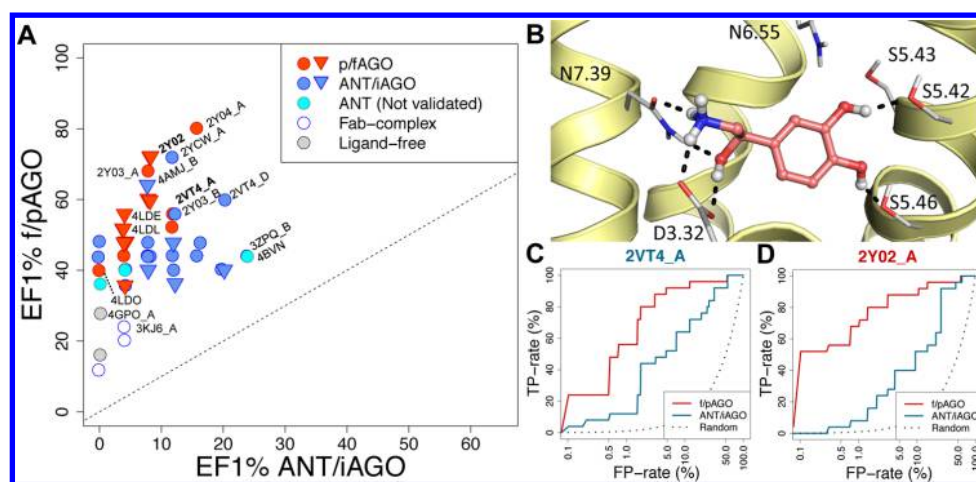
Figure 6. EF1% results for agonists and antagonists (A) when using the reference IFP of docked norepinephrine (Figure 2) in 2Y03_A (B). The individual ROC plots for the retrieval of agonists (red curve) and antagonists (blue curve) in the selected ANT/iAGO structure 2VT4_A (C) and f/pAGO structure 2Y02_A (D). Icons represent f/pAGO (red), ANT/iAGO (blue), or unvalidated ANT[34] (cyan) with no or unknown signaling preference (circle) or β-arrestin-biased ligands (triangle) (see Table 1).

iAGO $EF_{1\%}$ value (= 4). This active-state structure was successfully used in a prospective VS study in which 26 new β_2R agonists were identified using a similar IFP scoring approach (based on 24 overlapping residues and 9 additional residues to define the binding pocket for docking and IFP scoring).[105] In Figure 3B,C the individual ROC plots are displayed for the retrieval of ANT/iAGO and f/pAGO over decoys by IFP similarity scoring of docking poses generated in the 2VT4 and 2Y02 complexes using the reference IFPs (Figures 2 and 5C) of the corresponding co-crystallized ligands. Figure 3B,C shows the high early and overall enrichment for ligands with the same functional effect of the co-crystallized ligand and much lower early and overall enrichment for ligands with a different functional effect.

By rescoring all the docking poses of the compounds that were docked in all 48 structures with the reference IFPs from the two selected structures, the impact of the reference IFP selection was investigated (Figure 5D,E). For the selected f/pAGO IFP (2Y02_A), 93% of all ligand–protein complexes (excluding the 2Y02 structures) yielded an equal or higher f/pAGO $EF_{1\%}$ than when using their own IFP, in 64% of all cases a lower ANT/iAGO $EF_{1\%}$, and for almost all ligand–protein complexes a higher f/pAGO $EF_{1\%}$ than ANT/iAGO $EF_{1\%}$ (Figure 5D, 89% of all cases). When using the selected ANT/iAGO IFP (2VT4_A) instead of the IFP of the co-crystallized ligand to rescore all docked compounds in the ligand–protein complexes, a higher ANT/iAGO $EF_{1\%}$ (80% of all cases), a lower f/pAGO $EF_{1\%}$ (51% of all cases), and a higher ANT/iAGO $EF_{1\%}$ than f/pAGO $EF_{1\%}$ (82% of all cases) was obtained (Figure 5E). In two cases the use of the selected ANT/iAGO IFP resulted in an even higher ANT/iAGO $EF_{1\%}$ than with its own structure, namely in combination with the structure of cyanopindolol-bound β_1R ($EF_{1\%}$ = 52, 2YCY_A) and timolol-bound β_1R ($EF_{1\%}$ = 60, 3D4S). This is an increase of 4 and 24 in ANT/iAGO $EF_{1\%}$ for the 2YCY_A and 3D4S structures, respectively, compared to the enrichment obtained with their native IFP. This was not observed for the selected f/pAGO IFP, as the combination with its own structure (2Y02_A) resulted in the highest f/pAGO $EF_{1\%}$ (= 84). The results for one of the Fab complexes (2R4S) were somewhat surprising, as the f/pAGO $EF_{1\%}$ in combination with the selected ANT/iAGO IFP was higher than with the selected f/

pAGO IFP (36 and 16, respectively). Combining this with the fact that this structure is missing 23 of the binding pocket residues (*vide supra*), it was even more surprising that these enrichment factors can be obtained when docking in a structure with only half of the binding pocket. This does, however, match the success of previously published VS studies using homology models without ECL2[106] and low-resolution homology models.[45] Overall, it is clear that the selection of the reference IFP is essential and can influence the enrichment as well as selectivity of the outcome of a VS study, regardless of which structure was used.

In order to separately quantify the impact of the structure on the enrichment values, we studied the effect of rescoring all docking poses in the selected two structures with all 39 reference IFPs (Figure 5F,G). The results of rescoring the docking poses in the 2 selected structures with all reference IFPs show similar trends as rescoring with the reference IFP of the selected complexes (Figure 5D,E). For the selected f/pAGO structure (2Y02_A, Figure 5F), we see a shift in the results toward the f/pAGO and the opposite for when using the selected structure (2VT4_A, Figure 5G). The observed effect is, however, less pronounced. When we compare the obtained enrichment factors, they are on average 38% lower for the selected structures than when using their IFP to rescore the docking poses.

Moreover, with the right IFP, the selectivity of a crystal structure can be shifted toward ligands with another functional effect than the co-crystallized ligand (Figure 5D,E); the opposite (shifting the selectivity for ligands with another functional effect than the reference IFP ligand by using the right structure) is less frequently and less prominently observed. The selection of the crystal structure does, however, clearly influence the extent to which the IFP to able to shift this selectivity and also the final enrichment values. Combined, these results indicate that the correct IFP is more crucial for obtaining selectivity as well as high enrichments than the structure, but they also indicate that the best results are obtained by finding the right combination of IFP and structure.

Selective Structure-Based Virtual Screening for Partial/Full Agonists with a Computationally Predicted Norepinephrine Interaction Fingerprint. From the f/pAGO and ANT/iAGO retrieval rates in all structures (Figure

4A,B), we can see that in particular the IFP of epinephrine (PDB code 4LDO) is able to *selectively* retrieve f/pAGO ligands in all structures (with an average f/pAGO and ANT/iAGO $EF_{1\%}$ = 43.6 and 9.4, respectively). This small endogenous agonist makes all key interactions with $D113^{3.32}$, $N312^{7.39}$, and $S203^{5.42}$ in β_2R (Figure 2). On the basis of this observation, we hypothesized that the IFP of an even smaller agonist that could also make all these interactions should also be highly effective for the retrieval of f/pAGO over ANT/iAGO in all structures. As the crystal structure of norepinephrine bound to β_1R or β_2R has not yet been resolved, we docked norepinephrine and used the docking pose (Figure 6B) with the highest IFP score (compared to the IFP of isoproterenol) to obtain the reference IFP for norepinephrine in β_1R (Figure 2).

Indeed, when using this computationally predicted IFP to rescore all docked compounds in *all* structures, we were able to retrieve f/pAGO ligands with a high efficiency (the average f/pAGO and ANT/iAGO $EF_{1\%}$ = 46 and 8, respectively, Figures 4A and 6). On average, the obtained f/pAGO $EF_{1\%}$ was almost twice as high compared to the 2Y02_A IFP (the IFP from the highest-scoring f/pAGO complex). It should be noted that this is mostly due to higher f/pAGO $EF_{1\%}$ in the ANT/iAGO structures. At the same time, a 20% lower ANT/iAGO $EF_{1\%}$ was obtained compared to the 2Y02_A IFP. Moreover, the ANT/iAGO structure that obtained the highest f/pAGO $EF_{1\%}$ with this IFP was a cyanopindolol-bound β_1R structure (2YCW_A, Figure 6A), which coincides with the slight contraction of the pocket and the low f/pAGO rmsd as previously determined (Figure 1C). Interestingly, also in combination with the selected ANT/iAGO structure (cyanopindolol-bound 2VT4_A) the norepinephrine IFP was able to obtain a high and selective retrieval rate for f/pAGO ($EF_{1\%}$ = 56 and 12 for f/pAGO and ANT/iAGO, respectively, Figure 6C). The norepinephrine IFP combined with the 2Y02_A structure resulted in a slightly reduced f/pAGO $EF_{1\%}$, but at the same time reduced the ANT/iAGO $EF_{1\%}$, thereby making the results much more selective (Figure 6D).

By using the IFP from a small compound that makes all key interactions, these key interactions are highly emphasized, yielding more selective results. Whenever a docking pose of a compound misses one or more of the key interactions present in the reference IFP, this immediately results in a relatively low IFP score.

Biased Signaling. G-protein-coupled receptors can signal via G-proteins as well as β-arrestins.[107] So-called biased ligands can induce a preference of the receptor for one pathway over the other, this in contrast to the "classical" view in which GPCR ligands are solely able to stimulate, block, or reduce the G-protein signaling activity.[108] An in-depth literature search learned that for 7 of the 19 co-crystallized ligands there is a record of β-arrestin-biased signaling (Table 1). Among them are bucindolol and carvedilol, two β-blockers that promote signaling via the β-arrestin pathway.[32] For another 7 of the 19 co-crystallized compounds, we consistently found one or more publications reporting that ligand signaling is *not* biased (Table 1). It should be noted that the 7 biased ligands are all, with the exception of alprenolol,[82] relatively large compounds (Figure 1, Table 1) that stretch from the major pocket (between TM3, 4, 5, and 6) into the minor pocket[59] (between TM1, 2, 3, and 7). One should also note that the signaling bias of compounds is not always consistently observed and reported (e.g., for cyanopindolol,[78,81–83] carvedilol,[32,78,79,82] dobutamine[78,84]) as the effect seems to be dependent on assay type and

conditions,[84,109] receptor-activation state,[86] and receptor subtype[78] (β_1 versus β_2). Moreover, even for well-known and frequently used ligands the insights regarding signaling preference are constantly changing.[109,110]

For 29 of the 50 ligands in the docking set, there have been publications describing their signaling bias (Figure S9).[32,52,78–83,107] However, for 11 of those 29 compounds the signaling bias has been inconsistently reported, for 15 there is only 1 source, and for only 3 compounds (epinephrine, fenoterol, isoetharine) the signaling bias has been consistently reported in 2 or more publications of which only one (isoetharine) has a (β-arrestin) signaling bias (Figure S9). This hampers the structural investigation of the molecular determinants for biased signaling, which calls for consistent experimental methods for the identification and characterization of the signaling bias of GPCR ligands.[108,111,112]

In an attempt to identify potential key interactions for β-arrestin-biased ligand, we grouped all IFPs (Figure 2) of both the reported 7 biased and the reported 7 unbiased ligands that were co-crystallized. Subsequently, we calculated the difference in abundance for each interaction with each pocket residue (Supporting Information, Figure S11). This highlighted four interactions that had a high abundance ($\geq$50%) and were unique for the biased ligands. Three of them are hydrophobic contacts, namely with $L101/H93^{2.64}$, $D200/D192^{45.51}$, and $V326/I309^{7.36}$, and the fourth is an aromatic stacking interaction (face-to-face or face-to-edge) with $W117/W109^{3.28}$. Interestingly, this last interaction was present for all biased ligands, except for alprenolol. This could indicate that the signaling bias for these ligands is (partially) due to the aromatic stacking with this tryptophan residue. Moreover, isoproterenol is a full agonist with no signaling bias (it is even used as unbiased reference ligand[113]), but when a hydroxybenzyl moiety is attached the ligand (hydroxybenzylisoproterenol, 4LDL) makes an aromatic interaction with $W^{3.28}$ and induces a β-arrestin signaling bias.[52] This is also in line with mutation studies of the homologous $W^{3.28}$ in the muscarinic M_2 receptor (also a member of the aminergic-GPCR family[114]) that changed the signaling preference of the receptor when stimulated by specific ligands.[115] Also the contacts with $L101/H93^{2.64}$, $D200/D192^{45.51}$, and $V326/I309^{7.36}$ as well as (water-mediated) hydrogen bonds with ECL2 (as found for bucindolol and carvedilol[32]) might play a role.[87,116] For smaller compounds like alprenolol[82] and isoetharine[79] (not co-crystallized), there might be a different mode of action. Soriano-Ursua et al.[7] extensively reviewed this topic and discussed the possibility of two binding sites (the orthosteric pocket and a secondary binding region between TM 2, 3, 6, and 7) that can either be (partially) targeted simultaneously by larger ligands or independently by smaller ligands. Liu et al.[83] proposed, based on ^{19}F NMR, that all β-arrestin-biased ligands impact the conformational states of TM7. This theory is supported by the high abundance of hydrophobic contacts with $V326/I309^{7.36}$. The mechanism of biased signaling is, however, not yet fully understood and requires further structural, experimental, and *in silico* research.[7,87,117]

■ CONCLUSIONS

Due to the outstanding progress in GPCR crystallography and the resulting diversity of β-adrenergic X-ray structures, we were able to investigate the impact of receptor conformation (including activation state) and reference ligand on the selective and effective retrieval of full/partial agonists versus

antagonist/inverse agonist in this β-adrenoceptor case study. By systematically analyzing the selectivity and enrichment of 1920 combinations of unique reference IFPs and X-ray monomers, we gained new insights in structure-based prediction of GPCR ligand function. IFP rescoring was shown to be essential in order to obtain high enrichment factors and at the same time a high selectivity. The reference IFP has been shown to be more important than the receptor conformation for the VS outcome. By using the correct f/pAGO reference IFP, it was shown to be possible to selectively retrieve agonists in ANT/iAGO structures. Moreover, even the activation state of the receptor did not seem to have a great impact, as f/pAGO structures in both states gave comparable results. In the end, it is the match between receptor conformation and (predicted) reference IFP that can yield optimal results. It should be taken into account that the β_1R and β_2R represent a unique case because of the amount of diverse crystal structures which are now available. However, GPCR ligand function prediction and function-selective screenings are now also becoming possible for a few other GPCRs, for which both f/pAGO- and ANT/iAGO-bound crystal structures are available (i.e., the A$_{2A}$,[18,118,119] M$_2$,[120,121] and P2Y$_{12}$[122,123] receptors). The use of predicted ligand binding modes (guided and/or validated by experimental data such a ligand SAR or receptor mutation studies) could, however, bridge this gap for receptors for which such structural information is not yet available. In the current study, the potential of such an approach is illustrated by the fact that the predicted IFP of the small full agonist norepinephrine gave the highest retrieval rate of agonists over antagonists for *all* structures.

The ultimate next step would be to predict the signaling bias of GPCR ligands. For this, the IFP analysis of ligands with a stimulus bias and the identified key interaction points (L101/H93[2.64], D200/D192[45.51], and V326/I309[7.36]) can be valuable starting points. However, the observed issues with regard to the consistent experimental identification and characterization of biased ligands are currently hampering the structural investigation of the molecular determinants for biased signaling.

Taken together, this study provides insights into an effective approach for the selective identification of ligands with a specific functional effect. Ultimately, this will allow medicinal chemists to move from optimizing ligand affinity to designing ligands with the desired signaling properties.

■ MATERIALS AND METHODS

Crystal Structures Retrieval and Preparation. All β-adrenergic crystal structures were downloaded from the PDB (last accession date, April 4, 2014; see Table 1).[124] Subsequently, all structures were superposed using MOE[125] based on the residues surrounding the ligands (Figure 1). On the basis of the initial superposed structures, all residues within 4.5 Å of any ligand were determined as being the pocket residues (a total of 47):

V90/M82[2.53], V94/V86[2.57], G98/G90[2.61], A99/A91[2.62], L101/H93[2.64], V102/I94[2.65], G105/K97[2.68], W107/W99, C114/C106[3.25], W117/W109[3.28], T118/T110[3.29], D121/D113[3.32], V122/V114[3.33], L123/L115[3.34], V125/V117[3.36], T126/T118[3.37], V172/T164[4.56], S173/S165[4.57], C198/C190[45.49], C199/C191[45.50], D200/D192[45.51], F201/F193[45.52], V202/F194[45.53], T203/T195[45.54], N204/N196[5.35], Y207/Y199[5.38], A208/A200[5.39], I209/I201[5.40], S211/S203[5.42], S212/S204[5.43], I214/V206[5.45], S215/S207[5.46], F216/F208[5.47], W303/W286[6.48], F306/F289[6.51], F307/F290[6.52], N310/N293[6.55], N313/H296[6.58],

V314/V297[6.59], D322/K305[7.32], F325/Y308[7.35], V326/I309[7.36], A327/L310[7.37], N329/N312[7.39], W330/W313[7.40], G332/G315[7.42], and Y333/Y315[7.43].

The first and second residue numbers refer to the Uniprot residue numbers of β_1R and β_2R, respectively, while the Ballesteros−Weinstein[126] and extracellular loop 2 (ECL2)[106] residue numbers are reported as superscript. An in-house protocol similar to the KLIFS protocol[127] was performed to align all β-adrenergic crystal structures based on the selected 47 pocket residues, protonate the structures, and separately extract the ligand, pocket, protein, and (if present) waters, ions, organometallics, and cofactors in MOL2 format. All structures were subsequently inspected using MOE, and when necessary the protein-hydroxyl groups were adjusted for optimal H-bonding between the co-crystallized ligand and the receptor.

Consideration of Alternative Ligand Ring Conformations in 3ZPQ. The ring conformation of the fragment-like arylpiperazine ligand 19 in chain B of the β_1R crystal structure (PDB code 3ZPQ) did not allow for the secondary amine in the piperazine moiety to interact with both N329[7.39] and D121[3.32] due to its twist conformation. We therefore redocked the co-crystallized ligand, allowing for all possible ring conformations, and selected the highest-ranking pose, which is in the more stable chair conformation[128] (named *3ZPQ_dock*, see Figure S6).

Pocket and Ligand Analyses. Pocket volumes were calculated using POVME[129] (version 1.1.0) with a grid spacing of 0.5 Å and a padding of 1.09 Å. The initial inclusion volume was generated on the basis of three spheres with a radius of 7.0 Å, of which the centers were based on the superposed co-crystallized ligands (blue volume in Figure S5). Rmsd values between the pockets from the crystal structures were calculated using MOE. Distance calculations within the quadruplet (formed by G98/G90[2.61], D121/D113[3.32], N329/N312[7.39], and S211/S203[5.42]) and the subsequent Z-score analyses were performed using an in-house script. The residues that form the quadruplet were selected on the basis of their location and function in the binding pocket: G[2.61] is opposite of S[5.42] (an important interaction point for polar groups, in particular for agonists), N[7.39] is opposite of D[3.32] (both are key interaction points for the ligand amine group), the N[7.39]/D[3.32] pair is perpendicular to the G[2.61]/S[5.42] pair (Figure S4), and all four residues are roughly positioned at the same height in the TM helices with respect to the membrane.

Compound Preparation and Docking. Twenty-six ligands (13 f/pAGO and 13 ANT/iAGO) and 980 decoy compounds were obtained from the Supporting Information accompanying the publication from de Graaf et al.[55] In total 24 additional β-adrenergic ligands (12 f/pAGO and 12 ANT/iAGO) were selected on the basis of the classification reported by Baker.[85,88] Molecular (2D) structures of all 50 ligands are shown in Figure S9, comprising 25 f/pAGO (Figure S9A) and 25 ANT/iAGO (Figure S9B). Additional annotations (including references) regarding the experimentally observed signaling bias of these ligands have also been integrated in Figure S9.

All compounds were prepared starting from the SMILES format by first protonating all compounds at physiological pH using Chemaxon's Calculator (version 5.1.4)[130] and were subsequently converted to MOL2 format using CORINA (version 3.49).[131,132] All molecular docking simulations were carried out in fivefold using PLANTS[104] (version 1.2) using the (default) ChemPLP scoring function, search speed 2, flipping of free ring corners enabled, and generating 99 poses for every

compound with a clustering rmsd of 1.0. The docking experiments were performed in fivefold in order to reduce the effect of the stochastic nature of PLANTS,[104] as the use of a stochastic algorithm (as used in multiple docking algorithms, e.g., PLANTS,[104] GOLD,[133] and QXP[134]) can result in different docking poses for the same compound when performing multiple docking runs.

The binding site was based on the center of carazolol in β_2R (PDB code 2RH1) with a binding-site radius of 15 Å, thereby covering all pocket residues (except for G105/K97[2.68], which is pointing away from the binding site). In total, 1030 compounds were docked in 48 β-adrenergic structures, yielding almost 24.5 million docking poses.

Interaction Fingerprint Calculation and Scoring. From the individual pockets and ligands that were extracted from the crystal structures, interactions fingerprints were calculated through application of the FingerPrintLib (version 2.2, downloaded from http://bioinfo-pharma.u-strasbg.fr, using OpenEye's OEChem Toolkit[41]).[65,135] All docking poses were post-processed with IFP by combining the docking poses with the consistent pocket residue selection as indicated earlier. The IFPs from all docking-poses were scored using all 40 reference IFPs, resulting in ~979 million IFP scores representing their interaction profile similarity (as calculated by the Tanimoto similarity coefficient).

Virtual Screening Assessment. On the basis of the PLANTS and IFP scores of all docking poses, the highest scoring docking poses according to each of the scoring methods were selected. The resulting hit lists were used to rank both the f/pAGO and the ANT/iAGO ligands as well as the decoys and determine the enrichment factor (EF$_x$, where x is the false-positive rate) for each reference IFP (or ChemPLP score) and docking structure combination. The EF was determined by dividing the true-positive rate (TP-rate, i.e., the percentage of f/pAGO and ANT/iAGO, respectively) at a 1% false-positive rate[136] (FP-rate, i.e., 1% of the decoys; see Figures 3 and 4A,B) by the false positive rate, i.e., EF$_x$ = TP-rate/FP-rate$_x$. This implementation of the enrichment factor used is not database dependent (in contrast to the more classical enrichment factor[137]) and reflects the early enrichment well.[137,138] A possible drawback of the use of this EF implementation is that, to the best of our knowledge, there is no statistically sound way available to estimate the analytical error (e.g., the confidence interval) for the enrichment factors obtained.[137]

All EFs were calculated, resulting in the EF$_{1\%}$ of 1968 scoring combinations (40 reference IFP scores and 1 PLANTS score combined with 48 structures) for both the ranking of f/pAGO and ANT/iAGO ligands (see Figure 5).[137,138]

ASSOCIATED CONTENT

Ⓢ Supporting Information

Pharmacological details of all co-crystallized ligands, additional analyses of the pockets from the β-adrenergic X-rays (rmsd, distances, pocket contraction, binding modes, volumes), additional IFP analyses (interaction frequency per pocket residue, cross-comparison), two conformations of arylpiperazine 19, the 2D chemical structures of all docked ligands, and a scatter plot describing the overall enrichment using the ChemPLP scoring function. This material is available free of charge via the Internet at http://pubs.acs.org.

AUTHOR INFORMATION

Corresponding Author

*E-mail: c.de.graaf@vu.nl.

Notes

The authors declare no competing financial interest.

REFERENCES

(1) Hopkins, A. L.; Groom, C. R. The Druggable Genome. *Nat. Rev. Drug Discovery* **2002**, *1*, 727−730.

(2) Shoichet, B. K.; Kobilka, B. K. Structure-Based Drug Screening for G-Protein-Coupled Receptors. *Trends Pharmacol. Sci.* **2012**, *33*, 268−272.

(3) Violin, J. D.; Lefkowitz, R. J. Beta-Arrestin-Biased Ligands at Seven-Transmembrane Receptors. *Trends Pharmacol. Sci.* **2007**, *28*, 416−422.

(4) Kenakin, T.; Miller, L. J. Seven Transmembrane Receptors as Shapeshifting Proteins: The Impact of Allosteric Modulation and Functional Selectivity on New Drug Discovery. *Pharmacol. Rev.* **2010**, *62*, 265−304.

(5) Kobilka, B. The Structural Basis of G-Protein-Coupled Receptor Signaling (Nobel Lecture). *Angew. Chem., Int. Ed.* **2013**, *52*, 6380−6388.

(6) Urban, J. D.; Clarke, W. P.; von Zastrow, M.; Nichols, D. E.; Kobilka, B.; Weinstein, H.; Javitch, J. A.; Roth, B. L.; Christopoulos, A.; Sexton, P. M.; Miller, K. J.; Spedding, M.; Mailman, R. B. Functional Selectivity and Classical Concepts of Quantitative Pharmacology. *J. Pharmacol. Exp. Ther.* **2007**, *320*, 1−13.

(7) Soriano-Ursua, M. A.; Trujillo-Ferrara, J. G.; Correa-Basurto, J.; Vilar, S. Recent Structural Advances of Beta1 and Beta2 Adrenoceptors Yield Keys for Ligand Recognition and Drug Design. *J. Med. Chem.* **2013**, *56*, 8207−8223.

(8) Shukla, A. K.; Singh, G.; Ghosh, E. Emerging Structural Insights into Biased Gpcr Signaling. *Trends Biochem. Sci.* **2014**, *39*, 594−602.

(9) Jacobson, K. A.; Costanzi, S. New Insights for Drug Design from the X-Ray Crystallographic Structures of G-Protein-Coupled Receptors. *Mol. Pharmacol.* **2012**, *82*, 361−371.

(10) Katritch, V.; Cherezov, V.; Stevens, R. C. Structure-Function of the G Protein-Coupled Receptor Superfamily. *Annu. Rev. Pharmacol. Toxicol.* **2013**, *53*, 531−556.

(11) Granier, S.; Kobilka, B. A New Era of Gpcr Structural and Chemical Biology. *Nat. Chem. Biol.* **2012**, *8*, 670−673.

(12) Venkatakrishnan, A. J.; Deupi, X.; Lebon, G.; Tate, C. G.; Schertler, G. F.; Babu, M. M. Molecular Signatures of G-Protein-Coupled Receptors. *Nature* **2013**, *494*, 185−194.

(13) Jianyi, Y.; Yang, Z. GPCR-EXP: A Database for Experimentally Solved Gpcr Structures, http://zhanglab.ccmb.med.umich.edu/GPCR-EXP/ (accessed March 30, 2014).

(14) Hollenstein, K.; Kean, J.; Bortolato, A.; Cheng, R. K.; Dore, A. S.; Jazayeri, A.; Cooke, R. M.; Weir, M.; Marshall, F. H. Structure of Class B Gpcr Corticotropin-Releasing Factor Receptor 1. *Nature* **2013**, *499*, 438−443.

(15) Siu, F. Y.; He, M.; de Graaf, C.; Han, G. W.; Yang, D.; Zhang, Z.; Zhou, C.; Xu, Q.; Wacker, D.; Joseph, J. S.; Liu, W.; Lau, J.;

Cherezov, V.; Katritch, V.; Wang, M. W.; Stevens, R. C. Structure of the Human Glucagon Class B G-Protein-Coupled Receptor. *Nature* 2013, *499*, 444−449.

(16) Wu, H.; Wang, C.; Gregory, K. J.; Han, G. W.; Cho, H. P.; Xia, Y.; Niswender, C. M.; Katritch, V.; Meiler, J.; Cherezov, V.; Conn, P. J.; Stevens, R. C. Structure of a Class C Gpcr Metabotropic Glutamate Receptor 1 Bound to an Allosteric Modulator. *Science* 2014, *344*, 58−64.

(17) Wang, C.; Wu, H.; Katritch, V.; Han, G. W.; Huang, X. P.; Liu, W.; Siu, F. Y.; Roth, B. L.; Cherezov, V.; Stevens, R. C. Structure of the Human Smoothened Receptor Bound to an Antitumour Agent. *Nature* 2013, *497*, 338−343.

(18) Rodriguez, D.; Gao, Z. G.; Moss, S. M.; Jacobson, K. A.; Carlsson, J. Molecular Docking Screening Using Agonist-Bound Gpcr Structures: Probing the a Adenosine Receptor. *J. Chem. Inf. Model.* 2015, *55*, 550−563.

(19) White, J. F.; Noinaj, N.; Shibata, Y.; Love, J.; Kloss, B.; Xu, F.; Gvozdenovic-Jeremic, J.; Shah, P.; Shiloach, J.; Tate, C. G.; Grisshammer, R. Structure of the Agonist-Bound Neurotensin Receptor. *Nature* 2012, *490*, 508−513.

(20) Weichert, D.; Kruse, A. C.; Manglik, A.; Hiller, C.; Zhang, C.; Hubner, H.; Kobilka, B. K.; Gmeiner, P. Covalent Agonists for Studying G Protein-Coupled Receptor Activation. *Proc. Natl. Acad. Sci. U.S.A.* 2014, *111*, 10744−10748.

(21) Cherezov, V.; Rosenbaum, D. M.; Hanson, M. A.; Rasmussen, S. G.; Thian, F. S.; Kobilka, T. S.; Choi, H. J.; Kuhn, P.; Weis, W. I.; Kobilka, B. K.; Stevens, R. C. High-Resolution Crystal Structure of an Engineered Human Beta2-Adrenergic G Protein-Coupled Receptor. *Science* 2007, *318*, 1258−1265.

(22) Rasmussen, S. G.; Choi, H. J.; Rosenbaum, D. M.; Kobilka, T. S.; Thian, F. S.; Edwards, P. C.; Burghammer, M.; Ratnala, V. R.; Sanishvili, R.; Fischetti, R. F.; Schertler, G. F.; Weis, W. I.; Kobilka, B. K. Crystal Structure of the Human Beta2 Adrenergic G-Protein-Coupled Receptor. *Nature* 2007, *450*, 383−387.

(23) Hanson, M. A.; Cherezov, V.; Griffith, M. T.; Roth, C. B.; Jaakola, V. P.; Chien, E. Y.; Velasquez, J.; Kuhn, P.; Stevens, R. C. A Specific Cholesterol Binding Site Is Established by the 2.8 a Structure of the Human Beta2-Adrenergic Receptor. *Structure* 2008, *16*, 897−905.

(24) Warne, T.; Serrano-Vega, M. J.; Baker, J. G.; Moukhametzianov, R.; Edwards, P. C.; Henderson, R.; Leslie, A. G.; Tate, C. G.; Schertler, G. F. Structure of a Beta1-Adrenergic G-Protein-Coupled Receptor. *Nature* 2008, *454*, 486−491.

(25) Bokoch, M. P.; Zou, Y.; Rasmussen, S. G.; Liu, C. W.; Nygaard, R.; Rosenbaum, D. M.; Fung, J. J.; Choi, H. J.; Thian, F. S.; Kobilka, T. S.; Puglisi, J. D.; Weis, W. I.; Pardo, L.; Prosser, R. S.; Mueller, L.; Kobilka, B. K. Ligand-Specific Regulation of the Extracellular Surface of a G-Protein-Coupled Receptor. *Nature* 2010, *463*, 108−112.

(26) Wacker, D.; Fenalti, G.; Brown, M. A.; Katritch, V.; Abagyan, R.; Cherezov, V.; Stevens, R. C. Conserved Binding Mode of Human Beta2 Adrenergic Receptor Inverse Agonists and Antagonist Revealed by X-Ray Crystallography. *J. Am. Chem. Soc.* 2010, *132*, 11443−11445.

(27) Moukhametzianov, R.; Warne, T.; Edwards, P. C.; Serrano-Vega, M. J.; Leslie, A. G.; Tate, C. G.; Schertler, G. F. Two Distinct Conformations of Helix 6 Observed in Antagonist-Bound Structures of a Beta1-Adrenergic Receptor. *Proc. Natl. Acad. Sci. U.S.A.* 2011, *108*, 8228−8232.

(28) Rasmussen, S. G.; Choi, H. J.; Fung, J. J.; Pardon, E.; Casarosa, P.; Chae, P. S.; Devree, B. T.; Rosenbaum, D. M.; Thian, F. S.; Kobilka, T. S.; Schnapp, A.; Konetzki, I.; Sunahara, R. K.; Gellman, S. H.; Pautsch, A.; Steyaert, J.; Weis, W. I.; Kobilka, B. K. Structure of a Nanobody-Stabilized Active State of the Beta(2) Adrenoceptor. *Nature* 2011, *469*, 175−180.

(29) Rasmussen, S. G.; DeVree, B. T.; Zou, Y.; Kruse, A. C.; Chung, K. Y.; Kobilka, T. S.; Thian, F. S.; Chae, P. S.; Pardon, E.; Calinski, D.; Mathiesen, J. M.; Shah, S. T.; Lyons, J. A.; Caffrey, M.; Gellman, S. H.; Steyaert, J.; Skiniotis, G.; Weis, W. I.; Sunahara, R. K.; Kobilka, B. K. Crystal Structure of the Beta2 Adrenergic Receptor-Gs Protein Complex. *Nature* 2011, *477*, 549−555.

(30) Rosenbaum, D. M.; Zhang, C.; Lyons, J. A.; Holl, R.; Aragao, D.; Arlow, D. H.; Rasmussen, S. G.; Choi, H. J.; Devree, B. T.; Sunahara, R. K.; Chae, P. S.; Gellman, S. H.; Dror, R. O.; Shaw, D. E.; Weis, W. I.; Caffrey, M.; Gmeiner, P.; Kobilka, B. K. Structure and Function of an Irreversible Agonist-Beta(2) Adrenoceptor Complex. *Nature* 2011, *469*, 236−240.

(31) Warne, T.; Moukhametzianov, R.; Baker, J. G.; Nehme, R.; Edwards, P. C.; Leslie, A. G.; Schertler, G. F.; Tate, C. G. The Structural Basis for Agonist and Partial Agonist Action on a Beta(1)-Adrenergic Receptor. *Nature* 2011, *469*, 241−244.

(32) Warne, T.; Edwards, P. C.; Leslie, A. G.; Tate, C. G. Crystal Structures of a Stabilized Beta1-Adrenoceptor Bound to the Biased Agonists Bucindolol and Carvedilol. *Structure* 2012, *20*, 841−849.

(33) Zou, Y.; Weis, W. I.; Kobilka, B. K. N-Terminal T4 Lysozyme Fusion Facilitates Crystallization of a G Protein Coupled Receptor. *PLoS One* 2012, *7*, No. e46039.

(34) Christopher, J. A.; Brown, J.; Dore, A. S.; Errey, J. C.; Koglin, M.; Marshall, F. H.; Myszka, D. G.; Rich, R. L.; Tate, C. G.; Tehan, B.; Warne, T.; Congreve, M. Biophysical Fragment Screening of the Beta1-Adrenergic Receptor: Identification of High Affinity Arylpiperazine Leads Using Structure-Based Drug Design. *J. Med. Chem.* 2013, *56*, 3446−3455.

(35) Huang, J.; Chen, S.; Zhang, J. J.; Huang, X. Y. Crystal Structure of Oligomeric Beta1-Adrenergic G Protein-Coupled Receptors in Ligand-Free Basal State. *Nat. Struct. Mol. Biol.* 2013, *20*, 419−425.

(36) Carlsson, J.; Coleman, R. G.; Setola, V.; Irwin, J. J.; Fan, H.; Schlessinger, A.; Sali, A.; Roth, B. L.; Shoichet, B. K. Ligand Discovery from a Dopamine D3 Receptor Homology Model and Crystal Structure. *Nat. Chem. Biol.* 2011, *7*, 769−778.

(37) Carlsson, J.; Yoo, L.; Gao, Z. G.; Irwin, J. J.; Shoichet, B. K.; Jacobson, K. A. Structure-Based Discovery of A2a Adenosine Receptor Ligands. *J. Med. Chem.* 2010, *53*, 3748−3755.

(38) de Graaf, C.; Kooistra, A. J.; Vischer, H. F.; Katritch, V.; Kuijer, M.; Shiroishi, M.; Iwata, S.; Shimamura, T.; Stevens, R. C.; de Esch, I. J.; Leurs, R. Crystal Structure-Based Virtual Screening for Fragment-Like Ligands of the Human Histamine H(1) Receptor. *J. Med. Chem.* 2011, *54*, 8195−8206.

(39) Katritch, V.; Jaakola, V. P.; Lane, J. R.; Lin, J.; Ijzerman, A. P.; Yeager, M.; Kufareva, I.; Stevens, R. C.; Abagyan, R. Structure-Based Discovery of Novel Chemotypes for Adenosine a(2a) Receptor Antagonists. *J. Med. Chem.* 2010, *53*, 1799−1809.

(40) Kolb, P.; Rosenbaum, D. M.; Irwin, J. J.; Fung, J. J.; Kobilka, B. K.; Shoichet, B. K. Structure-Based Discovery of Beta2-Adrenergic Receptor Ligands. *Proc. Natl. Acad. Sci. U.S.A.* 2009, *106*, 6843−6848.

(41) Mysinger, M. M.; Weiss, D. R.; Ziarek, J. J.; Gravel, S.; Doak, A. K.; Karpiak, J.; Heveker, N.; Shoichet, B. K.; Volkman, B. F. Structure-Based Ligand Discovery for the Protein-Protein Interface of Chemokine Receptor Cxcr4. *Proc. Natl. Acad. Sci. U.S.A.* 2012, *109*, 5517−5522.

(42) de Graaf, C.; Rognan, D. Customizing G Protein-Coupled Receptor Models for Structure-Based Virtual Screening. *Curr. Pharm. Des.* 2009, *15*, 4026−4048.

(43) Kooistra, A. J.; Roumen, L.; Leurs, R.; de Esch, I. J.; de Graaf, C. From Heptahelical Bundle to Hits from the Haystack: Structure-Based Virtual Screening for GPCR Ligands. *Methods Enzymol.* 2013, *522*, 279−336.

(44) Palczewski, K.; Kumasaka, T.; Hori, T.; Behnke, C. A.; Motoshima, H.; Fox, B. A.; Le Trong, I.; Teller, D. C.; Okada, T.; Stenkamp, R. E.; Yamamoto, M.; Miyano, M. Crystal Structure of Rhodopsin: A G Protein-Coupled Receptor. *Science* 2000, *289*, 739−745.

(45) de Graaf, C.; Rein, C.; Piwnica, D.; Giordanetto, F.; Rognan, D. Structure-Based Discovery of Allosteric Modulators of Two Related Class B G-Protein-Coupled Receptors. *ChemMedChem* 2011, *6*, 2159−2169.

(46) Kellenberger, E.; Springael, J. Y.; Parmentier, M.; Hachet-Haas, M.; Galzi, J. L.; Rognan, D. Identification of Nonpeptide Ccr5 Receptor Agonists by Structure-Based Virtual Screening. *J. Med. Chem.* 2007, *50*, 1294−1303.

(47) Kiss, R.; Kiss, B.; Konczol, A.; Szalai, F.; Jelinek, I.; Laszlo, V.; Noszal, B.; Falus, A.; Keseru, G. M. Discovery of Novel Human Histamine H4 Receptor Ligands by Large-Scale Structure-Based Virtual Screening. *J. Med. Chem.* **2008**, *51*, 3145−3153.

(48) Salo, O. M.; Raitio, K. H.; Savinainen, J. R.; Nevalainen, T.; Lahtela-Kakkonen, M.; Laitinen, J. T.; Jarvinen, T.; Poso, A. Virtual Screening of Novel Cb2 Ligands Using a Comparative Model of the Human Cannabinoid Cb2 Receptor. *J. Med. Chem.* **2005**, *48*, 7166−7171.

(49) Tikhonova, I. G.; Sum, C. S.; Neumann, S.; Engel, S.; Raaka, B. M.; Costanzi, S.; Gershengorn, M. C. Discovery of Novel Agonists and Antagonists of the Free Fatty Acid Receptor 1 (Ffar1) Using Virtual Screening. *J. Med. Chem.* **2008**, *51*, 625−633.

(50) Varady, J.; Wu, X.; Fang, X.; Min, J.; Hu, Z.; Levant, B.; Wang, S. Molecular Modeling of the Three-Dimensional Structure of Dopamine 3 (D3) Subtype Receptor: Discovery of Novel and Potent D3 Ligands through a Hybrid Pharmacophore- and Structure-Based Database Searching Approach. *J. Med. Chem.* **2003**, *46*, 4377−4392.

(51) Kooistra, A. J.; Leurs, R.; de Esch, I. J.; de Graaf, C. From Three-Dimensional GPCR Structure to Rational Ligand Discovery. *Adv. Exp. Med. Biol.* **2014**, *796*, 129−157.

(52) Weiss, D. R.; Ahn, S.; Sassano, M. F.; Kleist, A.; Zhu, X.; Strachan, R.; Roth, B. L.; Lefkowitz, R. J.; Shoichet, B. K. Conformation Guides Molecular Efficacy in Docking Screens of Activated Beta-2 Adrenergic G Protein Coupled Receptor. *ACS Chem. Biol.* **2013**, *8*, 1018−1026.

(53) Moitessier, N.; Englebienne, P.; Lee, D.; Lawandi, J.; Corbeil, C. R. Towards the Development of Universal, Fast and Highly Accurate Docking/Scoring Methods: A Long Way to Go. *Br. J. Pharmacol.* **2008**, *153* (Suppl 1), S7−26.

(54) Sabio, M.; Jones, K.; Topiol, S. Use of the X-Ray Structure of the Beta2-Adrenergic Receptor for Drug Discovery. Part 2: Identification of Active Compounds. *Bioorg. Med. Chem. Lett.* **2008**, *18*, 5391−5395.

(55) de Graaf, C.; Rognan, D. Selective Structure-Based Virtual Screening for Full and Partial Agonists of the Beta2 Adrenergic Receptor. *J. Med. Chem.* **2008**, *51*, 4978−4985.

(56) Katritch, V.; Reynolds, K. A.; Cherezov, V.; Hanson, M. A.; Roth, C. B.; Yeager, M.; Abagyan, R. Analysis of Full and Partial Agonists Binding to Beta2-Adrenergic Receptor Suggests a Role of Transmembrane Helix V in Agonist-Specific Conformational Changes. *J. Mol. Recognit.* **2009**, *22*, 307−318.

(57) Reynolds, K. A.; Katritch, V.; Abagyan, R. Identifying Conformational Changes of the Beta(2) Adrenoceptor That Enable Accurate Prediction of Ligand/Receptor Interactions and Screening for Gpcr Modulators. *J. Comput. Aided Mol. Des.* **2009**, *23*, 273−288.

(58) Vilar, S.; Karpiak, J.; Berk, B.; Costanzi, S. In Silico Analysis of the Binding of Agonists and Blockers to the Beta2-Adrenergic Receptor. *J. Mol. Graph. Model.* **2011**, *29*, 809−817.

(59) Kooistra, A. J.; Kuhne, S.; de Esch, I. J.; Leurs, R.; de Graaf, C. A Structural Chemogenomics Analysis of Aminergic Gpcrs: Lessons for Histamine Receptor Ligand Design. *Br. J. Pharmacol.* **2013**, *170*, 101−126.

(60) Strader, C. D.; Candelore, M. R.; Hill, W. S.; Sigal, I. S.; Dixon, R. A. Identification of Two Serine Residues Involved in Agonist Activation of the Beta-Adrenergic Receptor. *J. Biol. Chem.* **1989**, *264*, 13572−13578.

(61) Kikkawa, H.; Kurose, H.; Isogaya, M.; Sato, Y.; Nagao, T. Differential Contribution of Two Serine Residues of Wild Type and Constitutively Active Beta2-Adrenoceptors to the Interaction with Beta2-Selective Agonists. *Br. J. Pharmacol.* **1997**, *121*, 1059−1064.

(62) Liapakis, G.; Ballesteros, J. A.; Papachristou, S.; Chan, W. C.; Chen, X.; Javitch, J. A. The Forgotten Serine. A Critical Role for Ser-2035.42 in Ligand Binding to and Activation of the Beta 2-Adrenergic Receptor. *J. Biol. Chem.* **2000**, *275*, 37779−37788.

(63) Sato, T.; Kobayashi, H.; Nagao, T.; Kurose, H. Ser203 as Well as Ser204 and Ser207 in Fifth Transmembrane Domain of the Human Beta2-Adrenoceptor Contributes to Agonist Binding and Receptor Activation. *Br. J. Pharmacol.* **1999**, *128*, 272−274.

(64) Ambrosio, C.; Molinari, P.; Cotecchia, S.; Costa, T. Catechol-Binding Serines of Beta(2)-Adrenergic Receptors Control the Equilibrium between Active and Inactive Receptor States. *Mol. Pharmacol.* **2000**, *57*, 198−210.

(65) Marcou, G.; Rognan, D. Optimizing Fragment and Scaffold Docking by Use of Molecular Interaction Fingerprints. *J. Chem. Inf. Model.* **2007**, *47*, 195−207.

(66) Verlinde, C. L.; Hol, W. G. Structure-Based Drug Design: Progress, Results and Challenges. *Structure* **1994**, *2*, 577−587.

(67) Jones, G.; Willett, P.; Glen, R. C.; Leach, A. R.; Taylor, R. Development and Validation of a Genetic Algorithm for Flexible Docking. *J. Mol. Biol.* **1997**, *267*, 727−748.

(68) Evers, A.; Klebe, G. Successful Virtual Screening for a Submicromolar Antagonist of the Neurokinin-1 Receptor Based on a Ligand-Supported Homology Model. *J. Med. Chem.* **2004**, *47*, 5381−5392.

(69) Barril, X.; Morley, S. D. Unveiling the Full Potential of Flexible Receptor Docking Using Multiple Crystallographic Structures. *J. Med. Chem.* **2005**, *48*, 4432−4443.

(70) Bissantz, C.; Bernard, P.; Hibert, M.; Rognan, D. Protein-Based Virtual Screening of Chemical Databases. Ii. Are Homology Models of G-Protein Coupled Receptors Suitable Targets? *Proteins* **2003**, *50*, 5−25.

(71) Katritch, V.; Rueda, M.; Abagyan, R. Ligand-Guided Receptor Optimization. *Methods Mol. Biol.* **2012**, *857*, 189−205.

(72) Tehan, B. G.; Bortolato, A.; Blaney, F. E.; Weir, M. P.; Mason, J. S. Unifying Family a Gpcr Theories of Activation. *Pharmacol. Ther.* **2014**, *143*, 51−60.

(73) Meng, X. Y.; Zhang, H. X.; Mezei, M.; Cui, M. Molecular Docking: A Powerful Approach for Structure-Based Drug Discovery. *Curr. Comput. Aided Drug Des.* **2011**, *7*, 146−157.

(74) Rognan, D.; Desaphy, J. Molecular Interaction Fingerprints. *Scaffold Hopping in Medicinal Chemistry*; Wiley-VCH Verlag GmbH & Co. KGaA: Weinheim, 2013; pp 215−230.

(75) Ring, A. M.; Manglik, A.; Kruse, A. C.; Enos, M. D.; Weis, W. I.; Garcia, K. C.; Kobilka, B. K. Adrenaline-Activated Structure of Beta2-Adrenoceptor Stabilized by an Engineered Nanobody. *Nature* **2013**, *502*, 575−579.

(76) Andrews, S. P.; Brown, G. A.; Christopher, J. A. Structure-Based and Fragment-Based Gpcr Drug Discovery. *ChemMedChem* **2014**, *9*, 256−275.

(77) Miller-Gallacher, J. L.; Nehme, R.; Warne, T.; Edwards, P. C.; Schertler, G. F.; Leslie, A. G.; Tate, C. G. The 2.1 a Resolution Structure of Cyanopindolol-Bound Beta1-Adrenoceptor Identifies an Intramembrane Na+ Ion That Stabilises the Ligand-Free Receptor. *PLoS One* **2014**, *9*, No. e92727.

(78) Casella, I.; Ambrosio, C.; Gro, M. C.; Molinari, P.; Costa, T. Divergent Agonist Selectivity in Activating Beta1- and Beta2-Adrenoceptors for G-Protein and Arrestin Coupling. *Biochem. J.* **2011**, *438*, 191−202.

(79) Drake, M. T.; Violin, J. D.; Whalen, E. J.; Wisler, J. W.; Shenoy, S. K.; Lefkowitz, R. J. Beta-Arrestin-Biased Agonism at the Beta2-Adrenergic Receptor. *J. Biol. Chem.* **2008**, *283*, 5669−5676.

(80) Kahsai, A. W.; Xiao, K.; Rajagopal, S.; Ahn, S.; Shukla, A. K.; Sun, J.; Oas, T. G.; Lefkowitz, R. J. Multiple Ligand-Specific Conformations of the Beta2-Adrenergic Receptor. *Nat. Chem. Biol.* **2011**, *7*, 692−700.

(81) Kaya, A. I.; Onaran, H. O.; Ozcan, G.; Ambrosio, C.; Costa, T.; Balli, S.; Ugur, O. Cell Contact-Dependent Functional Selectivity of Beta2-Adrenergic Receptor Ligands in Stimulating Camp Accumulation and Extracellular Signal-Regulated Kinase Phosphorylation. *J. Biol. Chem.* **2012**, *287*, 6362−6374.

(82) Kim, I. M.; Tilley, D. G.; Chen, J.; Salazar, N. C.; Whalen, E. J.; Violin, J. D.; Rockman, H. A. Beta-Blockers Alprenolol and Carvedilol Stimulate Beta-Arrestin-Mediated Egfr Transactivation. *Proc. Natl. Acad. Sci. U.S.A.* **2008**, *105*, 14555−14560.

(83) Liu, J. J.; Horst, R.; Katritch, V.; Stevens, R. C.; Wuthrich, K. Biased Signaling Pathways in Beta2-Adrenergic Receptor Characterized by 19f-Nmr. *Science* **2012**, *335*, 1106−1110.

(84) Rajagopal, S.; Ahn, S.; Rominger, D. H.; Gowen-MacDonald, W.; Lam, C. M.; Dewire, S. M.; Violin, J. D.; Lefkowitz, R. J. Quantifying Ligand Bias at Seven-Transmembrane Receptors. *Mol. Pharmacol.* 2011, *80*, 367−377.

(85) Baker, J. G. The Selectivity of Beta-Adrenoceptor Agonists at Human Beta1-, Beta2- and Beta3-Adrenoceptors. *Br. J. Pharmacol.* 2010, *160*, 1048−1061.

(86) Maack, C.; Bohm, M.; Vlaskin, L.; Dabew, E.; Lorenz, K.; Schafers, H. J.; Lohse, M. J.; Engelhardt, S. Partial Agonist Activity of Bucindolol Is Dependent on the Activation State of the Human Beta1-Adrenergic Receptor. *Circulation* 2003, *108*, 348−353.

(87) Warne, T.; Tate, C. G. The Importance of Interactions with Helix 5 in Determining the Efficacy of Beta-Adrenoceptor Ligands. *Biochem. Soc. Trans.* 2013, *41*, 159−165.

(88) Baker, J. G. The Selectivity of Beta-Adrenoceptor Antagonists at the Human Beta1, Beta2 and Beta3 Adrenoceptors. *Br. J. Pharmacol.* 2005, *144*, 317−322.

(89) Selvam, B.; Wereszczynski, J.; Tikhonova, I. G. Comparison of Dynamics of Extracellular Accesses to the Beta(1) and Beta(2) Adrenoceptors Binding Sites Uncovers the Potential of Kinetic Basis of Antagonist Selectivity. *Chem. Biol. Drug Des.* 2012, *80*, 215−226.

(90) Sheftel, S.; Muratore, K. E.; Black, M.; Costanzi, S. Graph Analysis of β_2 Adrenergic Receptor Structures: A "Social Network" of GPCR Residues. *In Silico Pharmacol.* 2013, DOI: 10.1186/2193-9616-1-16.

(91) Sato, M.; Hirokawa, T. Extended Template-Based Modeling and Evaluation Method Using Consensus of Binding Mode of Gpcrs for Virtual Screening. *J. Chem. Inf. Model.* 2014, *54*, 3153−3161.

(92) Deng, Z.; Chuaqui, C.; Singh, J. Structural Interaction Fingerprint (Sift): A Novel Method for Analyzing Three-Dimensional Protein-Ligand Binding Interactions. *J. Med. Chem.* 2004, *47*, 337−344.

(93) Desaphy, J.; Raimbaud, E.; Ducrot, P.; Rognan, D. Encoding Protein-Ligand Interaction Patterns in Fingerprints and Graphs. *J. Chem. Inf. Model.* 2013, *53*, 623−637.

(94) Venhorst, J.; Nunez, S.; Terpstra, J. W.; Kruse, C. G. Assessment of Scaffold Hopping Efficiency by Use of Molecular Interaction Fingerprints. *J. Med. Chem.* 2008, *51*, 3222−3229.

(95) Jansen, C.; Wang, H.; Kooistra, A. J.; de Graaf, C.; Orrling, K. M.; Tenor, H.; Seebeck, T.; Bailey, D.; de Esch, I. J.; Ke, H.; Leurs, R. Discovery of Novel Trypanosoma Brucei Phosphodiesterase B1 Inhibitors by Virtual Screening against the Unliganded Tbrpdeb1 Crystal Structure. *J. Med. Chem.* 2013, *56*, 2087−2096.

(96) Mpamhanga, C. P.; Spinks, D.; Tulloch, L. B.; Shanks, E. J.; Robinson, D. A.; Collie, I. T.; Fairlamb, A. H.; Wyatt, P. G.; Frearson, J. A.; Hunter, W. N.; Gilbert, I. H.; Brenk, R. One Scaffold, Three Binding Modes: Novel and Selective Pteridine Reductase 1 Inhibitors Derived from Fragment Hits Discovered by Virtual Screening. *J. Med. Chem.* 2009, *52*, 4454−4465.

(97) Richter, L.; de Graaf, C.; Sieghart, W.; Varagic, Z.; Morzinger, M.; de Esch, I. J.; Ecker, G. F.; Ernst, M. Diazepam-Bound Gabaa Receptor Models Identify New Benzodiazepine Binding-Site Ligands. *Nat. Chem. Biol.* 2012, *8*, 455−464.

(98) Daval, S. B.; Kellenberger, E.; Bonnet, D.; Utard, V.; Galzi, J. L.; Ilien, B. Exploration of the Orthosteric/Allosteric Interface in Human M1Muscarinic Receptors by Bitopic Fluorescent Ligands. *Mol. Pharmacol.* 2013, *84*, 71−85.

(99) Istyastono, E. P.; Kooistra, A. J.; Vischer, H. F.; Kuijer, M.; Roumen, L.; Nijmeijer, S.; Smits, R. A.; de Esch, I. J.; Leurs, R.; de Graaf, C. Structure-based virtual screening for fragment- like ligands of the G protein-coupled histamine H$_4$ receptor. *Med. Chem Commun.* 2015, DOI: 10.1039/C5MD00022J.

(100) Weis, W. I.; Kobilka, B. K. Structural Insights into G-Protein-Coupled Receptor Activation. *Curr. Opin. Struct. Biol.* 2008, *18*, 734−740.

(101) Petrongolo, C.; Macchia, B.; Macchia, F.; Martinelli, A. Molecular Orbital Studies on the Mechanism of Drug-Receptor Interaction. 2. Beta-Adrenergic Drugs. An Approach to Explain the Role of the Aromatic Moiety. *J. Med. Chem.* 1977, *20*, 1645−1653.

(102) Swaminath, G.; Xiang, Y.; Lee, T. W.; Steenhuis, J.; Parnot, C.; Kobilka, B. K. Sequential Binding of Agonists to the Beta2 Adrenoceptor. Kinetic Evidence for Intermediate Conformational States. *J. Biol. Chem.* 2004, *279*, 686−691.

(103) Strader, C. D.; Candelore, M. R.; Hill, W. S.; Dixon, R. A.; Sigal, I. S. A Single Amino Acid Substitution in the Beta-Adrenergic Receptor Promotes Partial Agonist Activity from Antagonists. *J. Biol. Chem.* 1989, *264*, 16470−16477.

(104) Korb, O.; Stutzle, T.; Exner, T. E. Empirical Scoring Functions for Advanced Protein-Ligand Docking with Plants. *J. Chem. Inf. Model.* 2009, *49*, 84−96.

(105) Kooistra, A. J.; Vischer, H. F.; McNaught-Flores, D. A.; De Esch, I. J. P.; Leurs, R.; de Graaf, C. Structure-Based Virtual Screening for Gpcr Ligands with a Specific Functional Effect, unpublished, 2014.

(106) de Graaf, C.; Foata, N.; Engkvist, O.; Rognan, D. Molecular Modeling of the Second Extracellular Loop of G-Protein Coupled Receptors and Its Implication on Structure-Based Virtual Screening. *Proteins* 2008, *71*, 599−620.

(107) Rajagopal, S.; Rajagopal, K.; Lefkowitz, R. J. Teaching Old Receptors New Tricks: Biasing Seven-Transmembrane Receptors. *Nat. Rev. Drug Discovery* 2010, *9*, 373−386.

(108) van der Westhuizen, E. T.; Breton, B.; Christopoulos, A.; Bouvier, M. Quantification of Ligand Bias for Clinically Relevant Beta2-Adrenergic Receptor Ligands: Implications for Drug Taxonomy. *Mol. Pharmacol.* 2014, *85*, 492−509.

(109) Reiner, S.; Ambrosio, M.; Hoffmann, C.; Lohse, M. J. Differential Signaling of the Endogenous Agonists at the Beta2-Adrenergic Receptor. *J. Biol. Chem.* 2010, *285*, 36188−36198.

(110) Copik, A. J.; Baldys, A.; Nguyen, K.; Sahdeo, S.; Ho, H.; Kosaka, A.; Dietrich, P. J.; Fitch, B.; Raymond, J. R.; Ford, A. P.; Button, D.; Milla, M. E. Isoproterenol Acts as a Biased Agonist of the Alpha-1a-Adrenoceptor That Selectively Activates the Mapk/Erk Pathway. *PLoS One* 2015, *10*, No. e0115701.

(111) Nijmeijer, S.; Vischer, H. F.; Sirci, F.; Schultes, S.; Engelhardt, H.; de Graaf, C.; Rosethorne, E. M.; Charlton, S. J.; Leurs, R. Detailed Analysis of Biased Histamine H(4) Receptor Signalling by Jnj 7777120 Analogues. *Br. J. Pharmacol.* 2013, *170*, 78−88.

(112) Nijmeijer, S.; Vischer, H. F.; Rosethorne, E. M.; Charlton, S. J.; Leurs, R. Analysis of Multiple Histamine H(4) Receptor Compound Classes Uncovers Galphai Protein- and Beta-Arrestin2-Biased Ligands. *Mol. Pharmacol.* 2012, *82*, 1174−1182.

(113) Galandrin, S.; Bouvier, M. Distinct Signaling Profiles of Beta1 and Beta2 Adrenergic Receptor Ligands toward Adenylyl Cyclase and Mitogen-Activated Protein Kinase Reveals the Pluridimensionality of Efficacy. *Mol. Pharmacol.* 2006, *70*, 1575−1584.

(114) Surgand, J. S.; Rodrigo, J.; Kellenberger, E.; Rognan, D. A Chemogenomic Analysis of the Transmembrane Binding Cavity of Human G-Protein-Coupled Receptors. *Proteins* 2006, *62*, 509−538.

(115) Gregory, K. J.; Sexton, P. M.; Tobin, A. B.; Christopoulos, A. Stimulus Bias Provides Evidence for Conformational Constraints in the Structure of a G Protein-Coupled Receptor. *J. Biol. Chem.* 2012, *287*, 37066−37077.

(116) Audet, M.; Bouvier, M. Insights into Signaling from the Beta2-Adrenergic Receptor Structure. *Nat. Chem. Biol.* 2008, *4*, 397−403.

(117) Costanzi, S. Modeling G Protein-Coupled Receptors in Complex with Biased Agonists. *Trends Pharmacol. Sci.* 2014, *35*, 277−283.

(118) Jaakola, V. P.; Griffith, M. T.; Hanson, M. A.; Cherezov, V.; Chien, E. Y.; Lane, J. R.; Ijzerman, A. P.; Stevens, R. C. The 2.6 Angstrom Crystal Structure of a Human A2a Adenosine Receptor Bound to an Antagonist. *Science* 2008, *322*, 1211−1217.

(119) Xu, F.; Wu, H.; Katritch, V.; Han, G. W.; Jacobson, K. A.; Gao, Z. G.; Cherezov, V.; Stevens, R. C. Structure of an Agonist-Bound Human A2a Adenosine Receptor. *Science* 2011, *332*, 322−327.

(120) Haga, K.; Kruse, A. C.; Asada, H.; Yurugi-Kobayashi, T.; Shiroishi, M.; Zhang, C.; Weis, W. I.; Okada, T.; Kobilka, B. K.; Haga, T.; Kobayashi, T. Structure of the Human M2Muscarinic Acetylcholine Receptor Bound to an Antagonist. *Nature* 2012, *482*, 547−551.

(121) Kruse, A. C.; Ring, A. M.; Manglik, A.; Hu, J.; Hu, K.; Eitel, K.; Hubner, H.; Pardon, E.; Valant, C.; Sexton, P. M.; Christopoulos, A.; Felder, C. C.; Gmeiner, P.; Steyaert, J.; Weis, W. I.; Garcia, K. C.; Wess, J.; Kobilka, B. K. Activation and Allosteric Modulation of a Muscarinic Acetylcholine Receptor. *Nature* **2013**, *504*, 101−106.

(122) Zhang, J.; Zhang, K.; Gao, Z. G.; Paoletta, S.; Zhang, D.; Han, G. W.; Li, T.; Ma, L.; Zhang, W.; Muller, C. E.; Yang, H.; Jiang, H.; Cherezov, V.; Katritch, V.; Jacobson, K. A.; Stevens, R. C.; Wu, B.; Zhao, Q. Agonist-Bound Structure of the Human P2y12 Receptor. *Nature* **2014**, *509*, 119−122.

(123) Zhang, K.; Zhang, J.; Gao, Z. G.; Zhang, D.; Zhu, L.; Han, G. W.; Moss, S. M.; Paoletta, S.; Kiselev, E.; Lu, W.; Fenalti, G.; Zhang, W.; Muller, C. E.; Yang, H.; Jiang, H.; Cherezov, V.; Katritch, V.; Jacobson, K. A.; Stevens, R. C.; Wu, B.; Zhao, Q. Structure of the Human P2y12 Receptor in Complex with an Antithrombotic Drug. *Nature* **2014**, *509*, 115−118.

(124) Bernstein, F. C.; Koetzle, T. F.; Williams, G. J.; Meyer, E. F., Jr.; Brice, M. D.; Rodgers, J. R.; Kennard, O.; Shimanouchi, T.; Tasumi, M. The Protein Data Bank: A Computer-Based Archival File for Macromolecular Structures. *J. Mol. Biol.* **1977**, *112*, 535−542.

(125) *Molecular Operating Environment (Moe)*, 2012.10; Chemical Computing Group Inc.: Montreal, Canada, 2012.

(126) Ballesteros, J. A.; Weinstein, H. Integrated Methods for the Construction of Three-Dimensional Models and Computational Probing of Structure-Function Relations of G Protein-Coupled Receptors. *Methods Neurosci.* **1995**, *25*, 366−428.

(127) van Linden, O. P.; Kooistra, A. J.; Leurs, R.; de Esch, I. J.; de Graaf, C. Klifs: A Knowledge-Based Structural Database to Navigate Kinase-Ligand Interaction Space. *J. Med. Chem.* **2014**, *57*, 249−277.

(128) Carey, F. A.; Sundberg, R. J. *Advanced Organic Chemistry: Part A: Structure and Mechanisms*. Springer: Berlin, 2007.

(129) Durrant, J. D.; de Oliveira, C. A.; McCammon, J. A. Povme: An Algorithm for Measuring Binding-Pocket Volumes. *J. Mol. Graph. Model.* **2011**, *29*, 773−776.

(130) *Calculator*, 5.1.4; ChemAxon Kft.: Budapest, Hungary.

(131) *Corina*, 3.4.9; Molecular Networks GmbH: Erlangen, Germany.

(132) Sadowski, J.; Gasteiger, J.; Klebe, G. Comparison of Automatic Three-Dimensional Model Builders Using 639 X-Ray Structures. *J. Chem. Inf. Comput. Sci.* **1994**, *34*, 1000−1008.

(133) Verdonk, M. L.; Cole, J. C.; Hartshorn, M. J.; Murray, C. W.; Taylor, R. D. Improved Protein-Ligand Docking Using Gold. *Proteins* **2003**, *52*, 609−623.

(134) McMartin, C.; Bohacek, R. S. Qxp: Powerful, Rapid Computer Algorithms for Structure-Based Drug Design. *J. Comput. Aided Mol. Des.* **1997**, *11*, 333−344.

(135) *Oechem Tk*, 1.7.2.4; OpenEye Scientific Software Inc.: Santa Fe, NM.

(136) Jain, A. N.; Nicholls, A. Recommendations for Evaluation of Computational Methods. *J. Comput. Aided Mol. Des.* **2008**, *22*, 133−139.

(137) Hawkins, P. C.; Warren, G. L.; Skillman, A. G.; Nicholls, A. How to Do an Evaluation: Pitfalls and Traps. *J. Comput. Aided Mol. Des.* **2008**, *22*, 179−190.

(138) Scior, T.; Bender, A.; Tresadern, G.; Medina-Franco, J. L.; Martinez-Mayorga, K.; Langer, T.; Cuanalo-Contreras, K.; Agrafiotis, D. K. Recognizing Pitfalls in Virtual Screening: A Critical Review. *J. Chem. Inf. Model.* **2012**, *52*, 867−881.